



---

## **APL DISDROMETER EVALUATION**

Jeffrey A. Nystuen  
John R. Proni  
Charles A. Lauter, Jr.  
Jeffrey Bufkin  
Ulises Rivero  
Mark Boland  
John C. Wilkerson

Atlantic Oceanographic and Meteorological Laboratory  
Miami, Florida  
December 1994

**APL DISDROMETER EVALUATION**

Jeffrey A. Nystuen  
John R. Proni  
Charles A. Lauter, Jr.  
Jeffrey Bufkin  
Ulises Rivero  
Mark Boland  
Ocean Acoustics Division  
Atlantic Oceanographic and Meteorological Laboratory

John C. Wilkerson  
Ocean Sciences Branch  
Satellite Research Laboratory  
Camp Springs, Maryland

Atlantic Oceanographic and Meteorological Laboratory  
Miami, Florida  
December 1994

**UNITED STATES  
DEPARTMENT OF COMMERCE**

**Ronald H. Brown  
Secretary**

**NATIONAL OCEANIC AND  
ATMOSPHERIC ADMINISTRATION**

**D. JAMES BAKER  
Under Secretary for Oceans  
and Atmosphere/Administrator**

Environmental Research  
Laboratories

James L. Rasmussen  
Director



## NOTICE

Mention of a commercial company or product does not constitute an endorsement by NOAA/ERL. Use of information from this publication concerning proprietary products or the tests of such products for publicity or advertising purposes is not authorized.

---

For sale by the National Technical Information Service, 5285 Port Royal Road  
Springfield, VA 22161

# CONTENTS

	<b>Page</b>
ABSTRACT .....	1
1. INTRODUCTION .....	1
2. BACKGROUND .....	2
A. The Joss-Waldvogel Disdrometer .....	2
B. The APL Disdrometer .....	2
3. REVIEW OF THE APL SYSTEM .....	2
4. SUGGESTED MODIFICATIONS TO THE APL CURCUIT: THE OAD CIRCUIT .....	5
5. COMPARISON OF APL AND OAD CIRCUITS .....	8
A. Dynamic Range .....	8
B. Temperature Sensitivity .....	16
C. Peak Detector .....	16
6. CALIBRATION .....	19
A. Synthetic Raindrop Production .....	19
B. Calibration Procedure .....	23
7. FIELD TESTS .....	23
A. Joss-Waldvogel Disdrometer Data .....	23
B. APL Disdrometer Data Processing .....	30
C. Data Comparison .....	31
8. CONCLUSIONS AND RECOMMENDATIONS .....	40
ACKNOWLEDGMENTS .....	40
APPENDIX A: APL CIRCUIT SOFTWARE .....	41
REFERENCES .....	43

# APL DISDROMETER EVALUATION

Jeffrey A. Nystuen, John R. Proni, Charles A. Lauter, Jr., Jeffrey Bufkin,  
Ulises Rivero, Mark Boland, and John C. Wilkerson

**ABSTRACT.** The Ocean Acoustics Division at the Atlantic Oceanographic and Meteorological Laboratory has evaluated a new disdrometer design developed by the Applied Physics Laboratory of John Hopkins University. Modified electronics have been added to the data processing circuitry to reduce temperature sensitivity and increase the dynamic range of the instrument. Calibration was performed using water drops from 0.6-5.5 mm diameter impacting the sensor head at terminal velocity. Field comparison to a Joss-Waldvogel disdrometer shows equal performance characteristics at low rainfall rates and slightly better performance for rainfall rates above 100 mm/hr. Engineering circuit design details and physical design of the calibration apparatus are described.

## 1. INTRODUCTION

A disdrometer measures the distribution of drop sizes within rain. It is used to support meteorological research in rain and cloud physics. It is particularly suited to interpreting and calibrating weather radar and other advanced rainfall measuring instruments including optical and acoustical rain gauges. These remote sensing instruments measure integrated high moments of the actual drop size distribution within the rain and then, usually, attempt to estimate the rainfall rate, a quantity proportional to the 3.6th moment of the drop size distribution. If the quantity measured does not have the same moment of the rain as rainfall rate, errors are likely (Ulbrich and Atlas, 1978). A measurement of the actual drop size distribution is, therefore, a critical component to understanding the performance of these instruments.

The National Oceanic and Atmospheric Administration (NOAA) Global Precipitation Climatology Project (GPCP) and the National Aeronautics and Space Administration (NASA) Tropical Rain Measuring Mission (TRMM) have a common interest in rainfall instrumentation and test-site development. In preparation for the TRMM satellite, NASA has identified several locations to serve as surface truth sites for calibration of the satellite-mounted sensors. These sites are to be equipped with the best possible rainfall measurement instruments, including disdrometers. Currently, only one disdrometer design, a RD-69 Distromet Disdrometer (Joss and Waldvogel, 1969), is commercially available. This unit is expensive and apparently susceptible to corrosion in marine environments. It is not deployable on ocean platforms. A more robust disdrometer was designed at the Applied Physics Laboratory (APL) of John Hopkins University (Rowland, 1976) based on an earlier design by Flach (1972). Consequently, GPCP and TRMM requested that a new prototype of the APL disdrometer be produced. Fourteen sensor heads and one electronics package were built.

The disdrometer evaluation is a joint effort of the Atlantic Oceanographic and Meteorological Laboratory (AOML/ERL) and the Satellite Research Laboratory (SRL/NESDIS). The Ocean Acoustics Division (OAD) at AOML/ERL has established a facility to evaluate the performance of a variety of automatically recording rain gauges (Nystuen *et al.*, 1995). Included within the OAD system is a Joss-Waldvogel disdrometer. Using the Joss-Waldvogel instrument as a comparison instrument, OAD was asked to review/modify the APL electronics package, and then calibrate and field test the modified disdrometer design. These new disdrometers are to be made available for the TRMM surface truth sites and appropriate GPCP projects.

## 2. BACKGROUND

Raindrops range in size from roughly 200  $\mu\text{m}$  to 6 mm in diameter (Pruppacher and Pitter, 1971). These drops have sufficient mass so that they fall to the surface rather than being held aloft by air currents. The terminal fall velocity of the drops is an increasing function of drop size (Figure 1). This relationship can be approximated by

$$V_T = 9.23 (1 - e^{-0.068D^3 - 4.88D})$$

where  $V_T$  is the terminal velocity (m/s) and  $D$  is the raindrop diameter (mm) (Lhermitte, 1990). As a consequence of this relationship, the total drop momentum is also an increasing function of drop size (Figure 2). Disdrometers convert the momentum of a raindrop striking the sensor head into an electrical pulse, which in turn can be related to the drop size.

### A. The Joss-Waldvogel Disdrometer

The Joss-Waldvogel disdrometer is an electro-mechanical instrument. The sensor consists of a light-weight styrofoam cone which moves when struck by a raindrop. The movement of the cone is sensed by an attached coil residing in a magnetic field. The voltage output from the sensing coil is amplified and used to drive another coil attached to the styrofoam cone. This second coil serves as a feedback to return the cone to its original position quickly, improving the response time of the sensor. Output from the feedback amplifier is applied to a signal processing circuit which compresses the signal and produces a voltage which is calibrated for drop size. In addition, this circuit senses the mean background voltage of the sensor and continually adjusts the threshold of the smallest measured drop size. In noisy environments, including heavy rainfall, the threshold of smallest drop detection can approach 1 mm diameter, *i.e.*, no drops below the threshold are detected. The sensor head material is very light weight and is easily dented or damaged.

### B. The APL Disdrometer

The APL disdrometer uses a piezoelectric transducer which is bonded to the bottom of a Delrin cylinder and set into a brass mounting. A raindrop striking the sensor head produces a resonance within the Delrin cylinder/brass mounting that is converted to voltage by the piezoelectric transducer. The damping rate of the sensor is a function of the dimensions of the cylinder and the brass mounting. This signal, a rapidly damped sine wave, is filtered, compressed, and demodulated within a demodulator circuit. In a computer interface circuit, the peak voltage is detected and digitized within a processing computer. This voltage value is calibrated to drop size. A minimum threshold has to be set within the computer interface circuit to avoid false triggering. Unlike the Joss-Waldvogel disdrometer, there is no automatic threshold modification within the circuit.

## 3. REVIEW OF THE APL SYSTEM

The sensor unit is very robust. Unlike the Joss-Waldvogel disdrometer, the sensor surface is made of Delrin and should not be damaged by accidental impact of hard objects. The plated brass mounting uses o-rings to prevent water from reaching the piezoelectric wafer. There are two openings in the base of the mounting which APL recommends be plugged. One is required for release of air during assembly of the sensor head and should be plugged. The second allows the wire leads to the piezoelectric wafer to exit the unit. It should be made water tight.

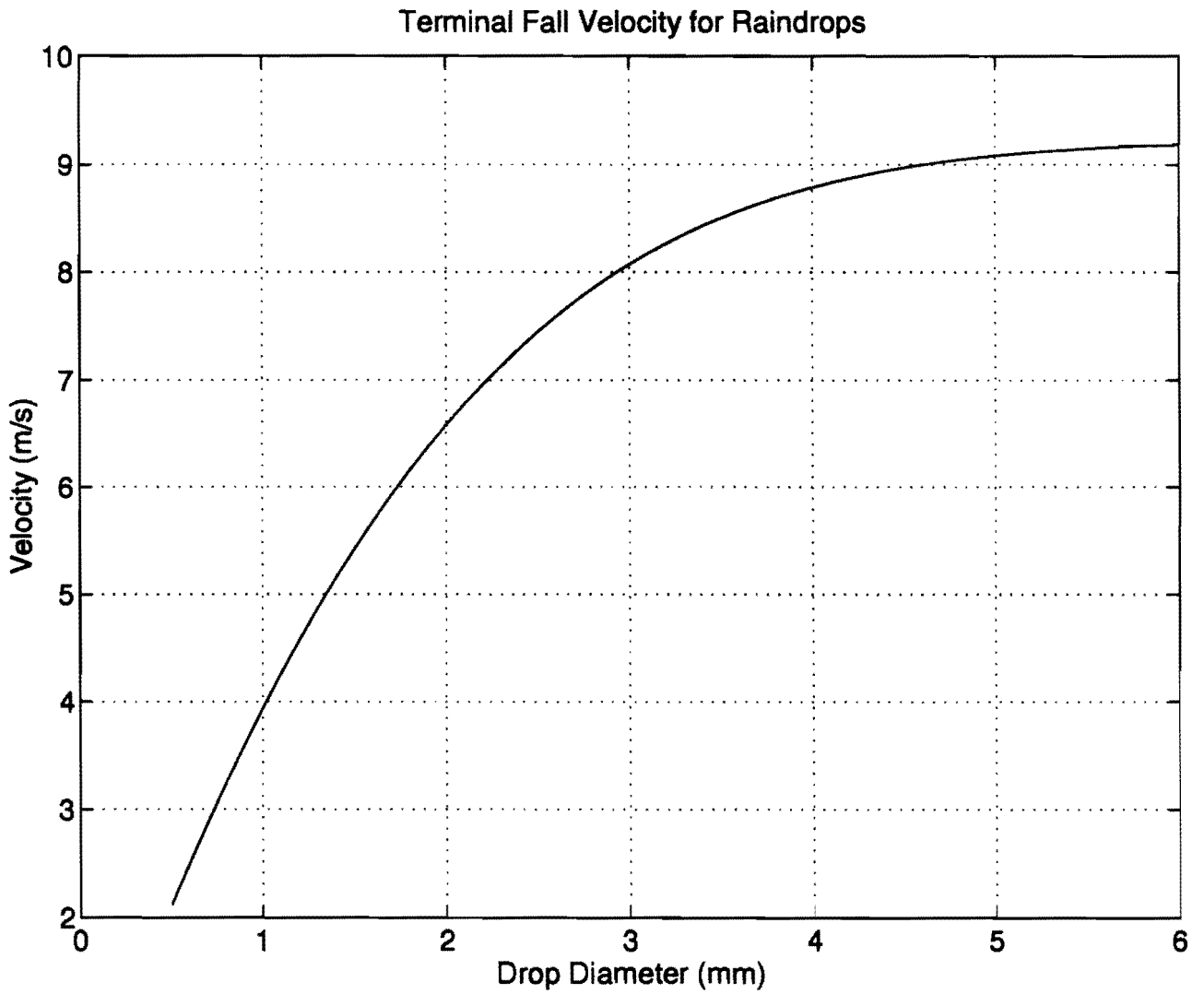


Figure 1. Terminal velocity for natural raindrops (Lhermitte, 1990).

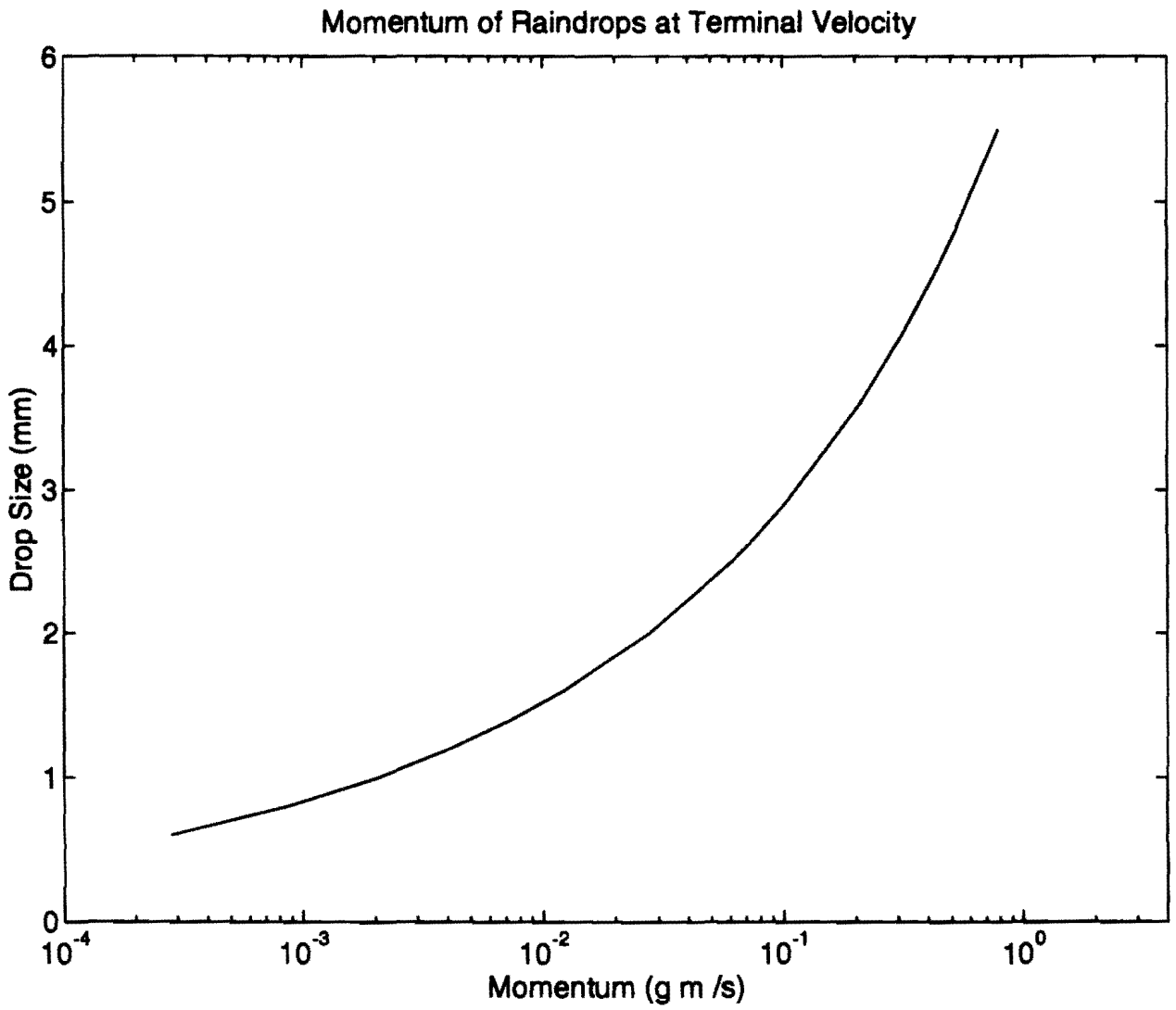


Figure 2. Momentum of raindrops at terminal velocity.

The APL electronic circuit consists of two submodules. The first submodule, the demodulator, is located near the sensor head via a short coaxial cable. This submodule converts the damped sine wave voltage signal into a demodulated pulse. This demodulated pulse is then sent to the computer interface module. The computer interface module is located near the recording computer and can be several hundred meters away from the demodulator unit. Within the computer interface module, a threshold detection circuit is applied. If the threshold level is exceeded, a peak detector tracks and then holds the highest value of the demodulated pulse. When the signal drops below the threshold level, a "data ready" interrupt is sent to the recording computer. The computer digitizes the peak level value (A/D conversion) and releases the peak detector unit, allowing the next drop to be recorded.

After testing the APL system at each step of the circuit, OAD engineers made several suggestions. Since the APL circuit was designed, new integrated circuits have become available. In particular, the Analog-Devices AD640 "DC Coupled Demodulating Logarithmic Amplifier" can be used to perform the amplification, compression, and demodulation of the demodulator unit. This chip has built-in temperature compensation for gain, transfer function, and DC drift.

A second change is in the peak detector of the computer interface submodule. The original peak detector, a Burr-Brown peak detector, is no longer commercially available. Inexpensive, high quality, commercially available peak detectors are available to perform the required function. Another change is to reduce the number of adjustment points within the circuit to two: the gain of the amplifier in the demodulator submodule and the threshold level in the interface submodule. Finally, the computer interface board contained circuitry for several auxiliary rain gauges (tipping bucket rain gauges). These instruments are not part of the disdrometer system and, thus, the extra circuitry can be removed.

#### **4. SUGGESTED MODIFICATIONS TO THE APL CIRCUIT: THE OAD CIRCUIT**

The overall philosophy of the APL circuit is preserved. Figure 3 shows a physical block diagram of the system. The changes occur within the demodulator unit and within the computer interface unit. The modified circuit will be referred to as the OAD circuit.

The function block diagram of the demodulator unit is shown in Figure 4. The principal changes in the demodulator unit are the two cascaded Analog-Devices AD640 IC chips. The AD640 is a "DC Coupled Demodulating Logarithmic Amplifier." Together, the two AD640s produce an output current that is accurately proportional to the log (base 10) of the input voltage over an input voltage range of 80 dB. Temperature compensation for gain, transfer function, and DC drift are built in. These are very wide band devices (over 100 MHz) that require the use of high frequency design techniques in layout and bypassing. For example, the use of a ground plane is required. All components are surface mounted.

In order to obtain the high gain needed to measure small raindrops, bandwidth limiting and filtering must be applied several places in the circuit. A simple low-pass RF filter is located at the input to the first stage (IC-1). The first stage (U1) is both an amplifier and an active filter. This filter has a low "Q" and a center frequency of about 3 kHz. The amplifier has an adjustable attenuator at its input. This attenuator (potentiometer) is the only adjustment in the demodulator circuit. Different disdrometer sensor heads will require that this attenuator be adjusted to produce equal output from the demodulator circuit. Capacitors C-4 and C-5, along with the output impedance of IC-2, low pass filter signals applied to transformer T-1. The transformer acts as a bandpass filter to further reduce noise in the signal applied to IC-3. The sum of the signal currents from IC-2 and IC-3 are the amplified, filtered, log compressed, and demodulated (unipolar) version of the rain impact signal. The currents from IC-2 and IC-3 are summed and converted to voltage and integrated by IC-4. This stage also integrates or smooths the signal to remove signal components and noise in the signal above 4 kHz. These signal components are mostly

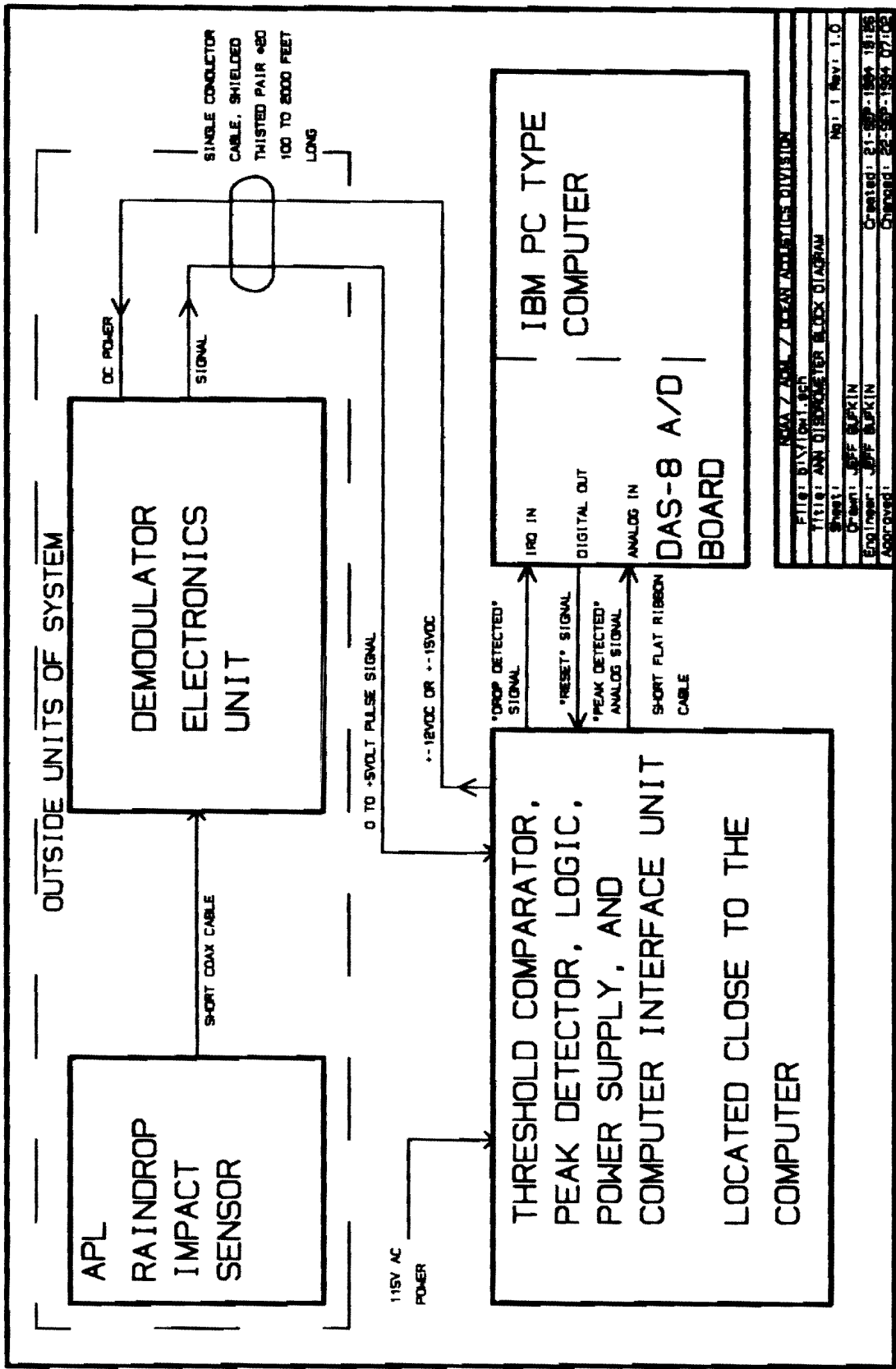


Figure 3. Block diagram of the OAD circuitry. This is unchanged from the APL circuitry.

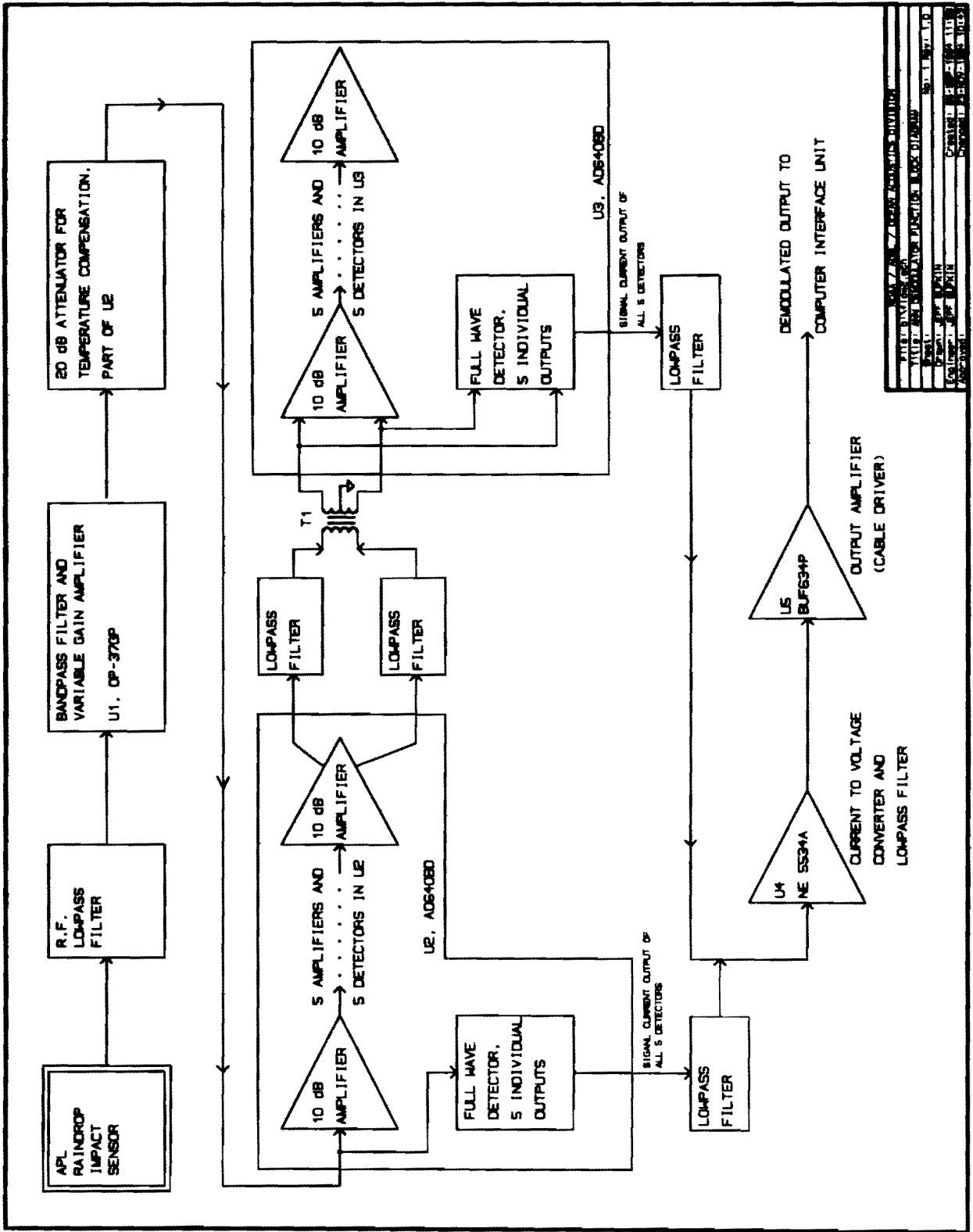


Figure 4. Block diagram of the OAD demodulator circuit.

harmonics of the sensor head. The output amplifier IC-5 can drive a long shielded/twisted pair cable. The engineering diagram for this unit is shown in Figure 5.

The computer interface submodule was modified by replacing the signal input stage with an instrumentation type amplifier to deal with common mode noise and to improve the precision of the gain. Furthermore, two adjustments are eliminated. The only remaining adjustment associated with this submodule is the threshold value for peak detection. The new peak detector unit is an Analog Devices P/N PKD01EP. The engineering diagram for the interface submodule is shown in Figure 6.

## 5. COMPARISON OF APL AND OAD CIRCUITS

After design changes were identified, a modified circuit, which will be referred to as the OAD circuit, was built. Comparison to the original APL circuit was conducted under identical conditions for both circuits. Tests included (a) pulse shape form (the output of the demodulator unit) using a full range of simulated raindrop sizes, (b) temperature sensitivity using a known input voltage, and (c) evaluation of three peak detector circuits: the Burr-Brown unit, an APL design, and a commercially available Analog Devices unit.

### A. Dynamic Range

An example of the damped sine wave signal from the sensor head is shown in Figure 7. The demodulator unit converts this signal to a filtered, compressed, and demodulated pulse that is sent to the computer interface unit. To compare the APL and OAD demodulator units, the signal produced by the largest synthetic raindrop size (a 5.5 mm drop impacting at terminal velocity) was adjusted to have equal peak voltage values (4.5 V) after demodulation. The signal from seven raindrop sizes ranging from 5.5-0.8 mm diameter were then examined. Figures 8-11 show the pulse shape exiting the demodulator circuits. Note that in Figure 8, the largest drop size, that the peak amplitude for the APL and OAD circuits is the same. This was intentional to allow later comparison at smaller drop sizes. The APL pulse has a sharper peak and decays more rapidly. There is some high frequency noise in the pulse shape; however, the only important characteristics are the peak value (detected by the peak detector), the time interval above the threshold, and the signal level to threshold level ratio (especially for small raindrops). Figure 9 shows the signal for a large drop size (3.6 mm). The signal from both units is similar to Figure 8. Figure 10 shows the signal for a 1.0 mm raindrop. Finally, the signal for the 0.8 mm drop, Figure 11, is 0.8 V in the OAD circuit but only 0.15 V in the APL circuit.

The operational measure of drop detection ability is the signal level to threshold level ratio (S/T). The threshold level was chosen to be the minimum voltage level required to suppress false triggering in the detection circuit by random noise in the laboratory. Using the OAD circuit,  $S/T \approx 6$  for a 1.0 mm drop and  $S/T \approx 3$  for a 0.8 mm drop, *i.e.*, 0.8 mm drops were reliably detected using the OAD circuit. In contrast, using the APL circuit,  $S/T \approx 2$  for a 1.0 mm drop and  $S/T \approx 1$  for 0.8 mm drops, *i.e.*, 0.8 mm drops could not be reliably detected using the APL circuit. Increasing the demodulator gain in the APL circuit did not improve this detection ability ratio (and did result in electronic clipping of the larger drop, *i.e.*, >3 mm diameter, signals). Thus, the increased dynamic range of the OAD circuit allowed consistent detection of smaller raindrops in laboratory testing.

Because of the extended dynamic range of the OAD demodulator, the time interval that a signal is above a given threshold is approximately 30% longer than for the APL demodulator.

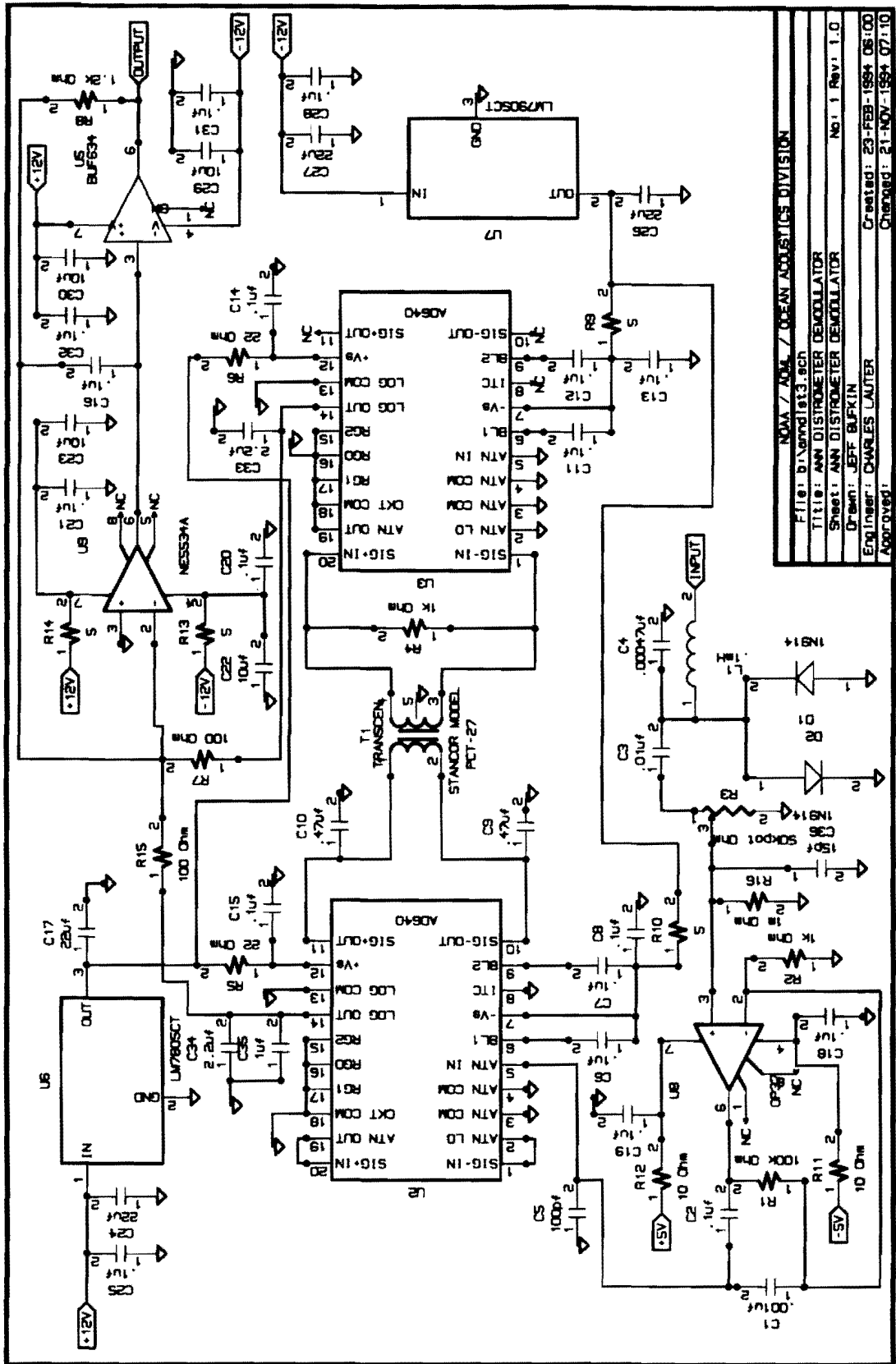
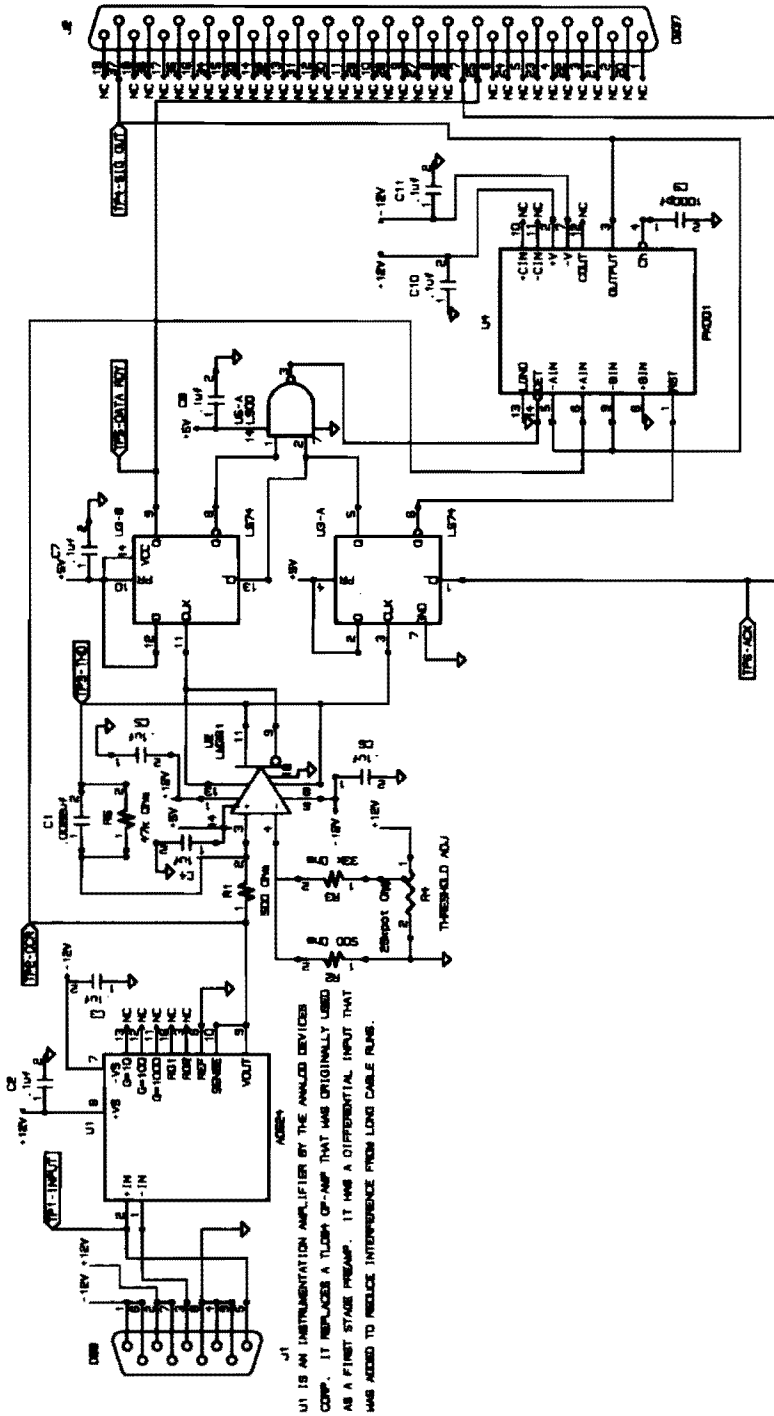


Figure 5. Electrical engineering design of the OAD demodulator circuit.



DATE	1987/08/27	DESIGN	SYSTEMS ENGINEER
TIME	10:00 AM	BY	W. L. BROWN, I.O.
PROJECT	OAD	NO.	1000
REVISION	1	DATE	1987/08/27
APPROVED	W. L. BROWN	DESIGNED	W. L. BROWN
INSTRUMENT	OAD	TESTED	W. L. BROWN
REVISION	1	DATE	1987/08/27

Figure 6. Electrical engineering design of the OAD computer interface circuit.

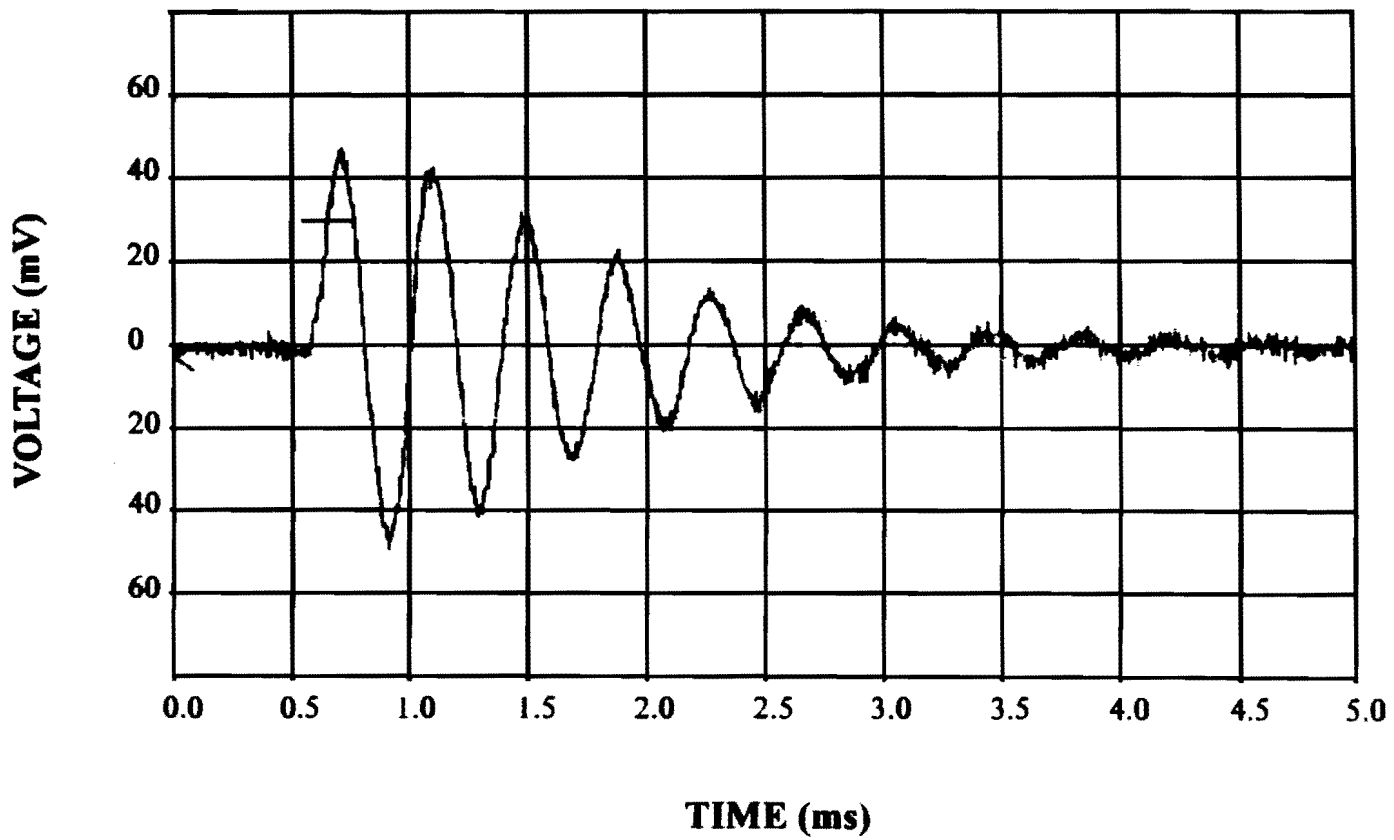


Figure 7. The damped sine wave signal from the Delrin sensor head.

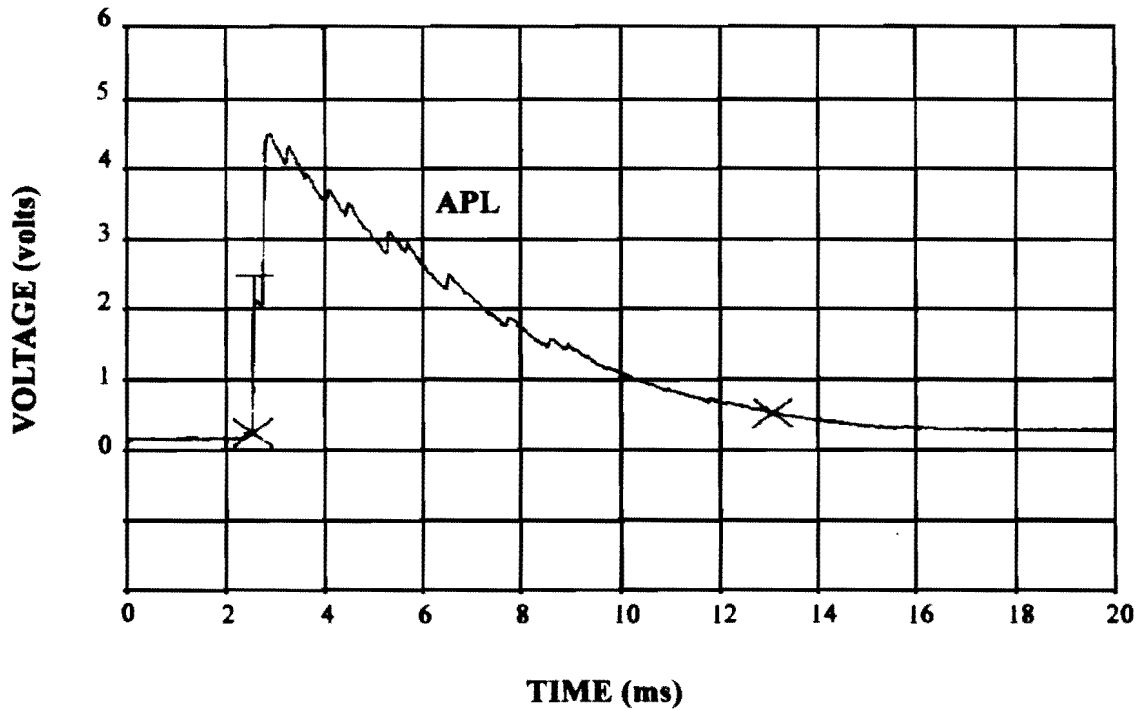
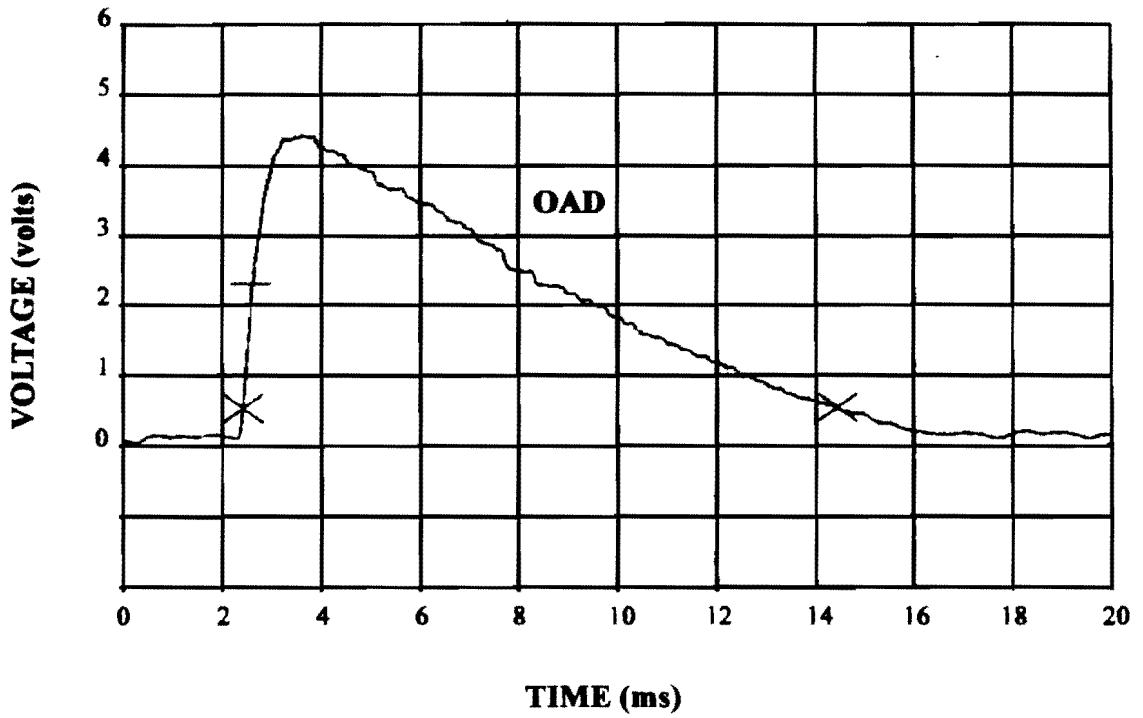


Figure 8. The demodulated signal of a 5.5 mm raindrop impact using the APL (top) and OAD (bottom) circuits. The APL and OAD circuit gains were adjusted so that this drop size (the largest used) gave equal output voltages.

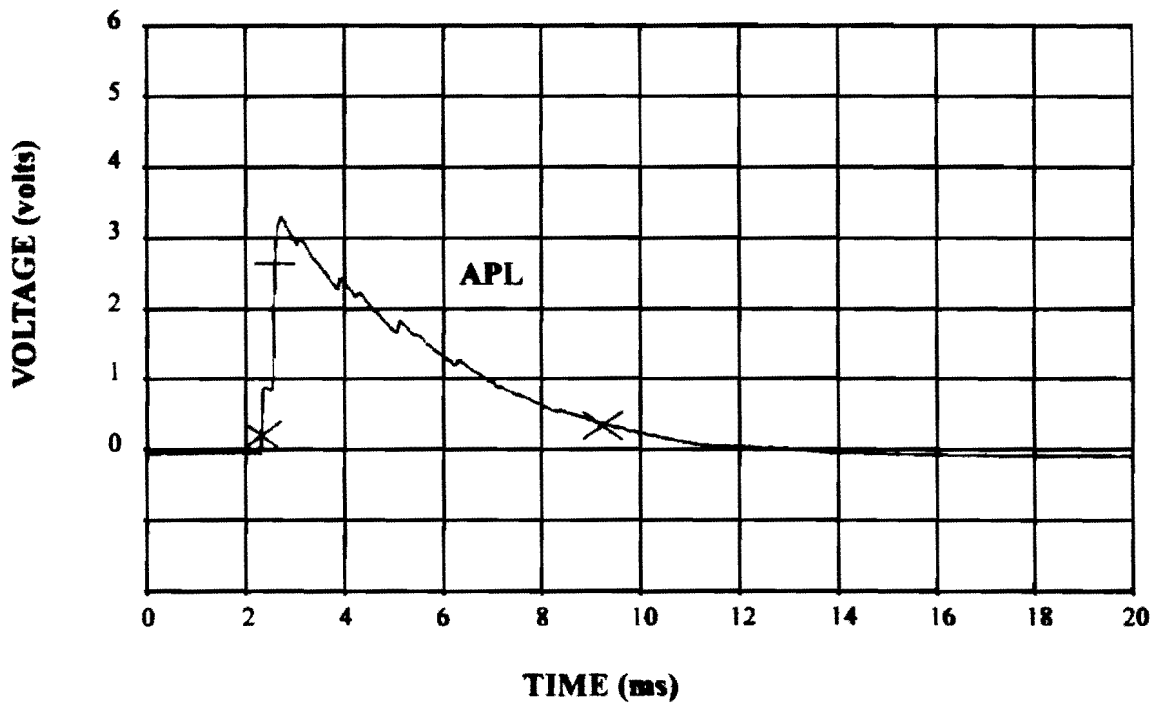
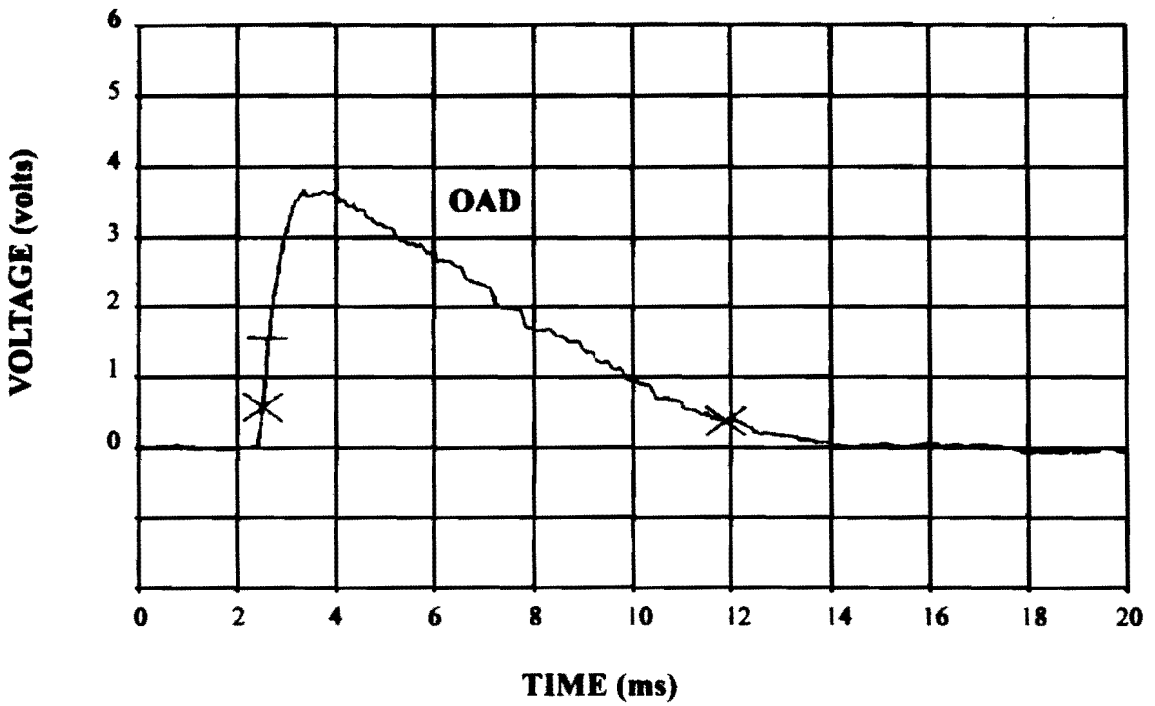


Figure 9. The demodulated signal of a 3.6 mm raindrop impact using the APL (top) and OAD (bottom) circuits.

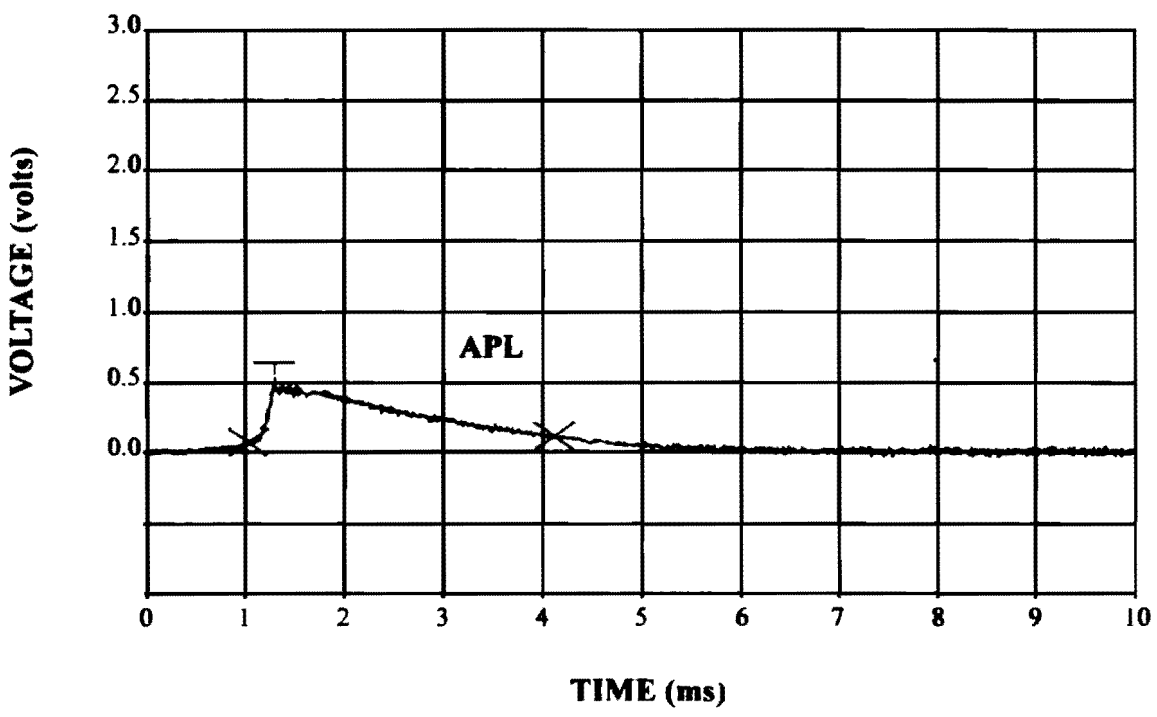
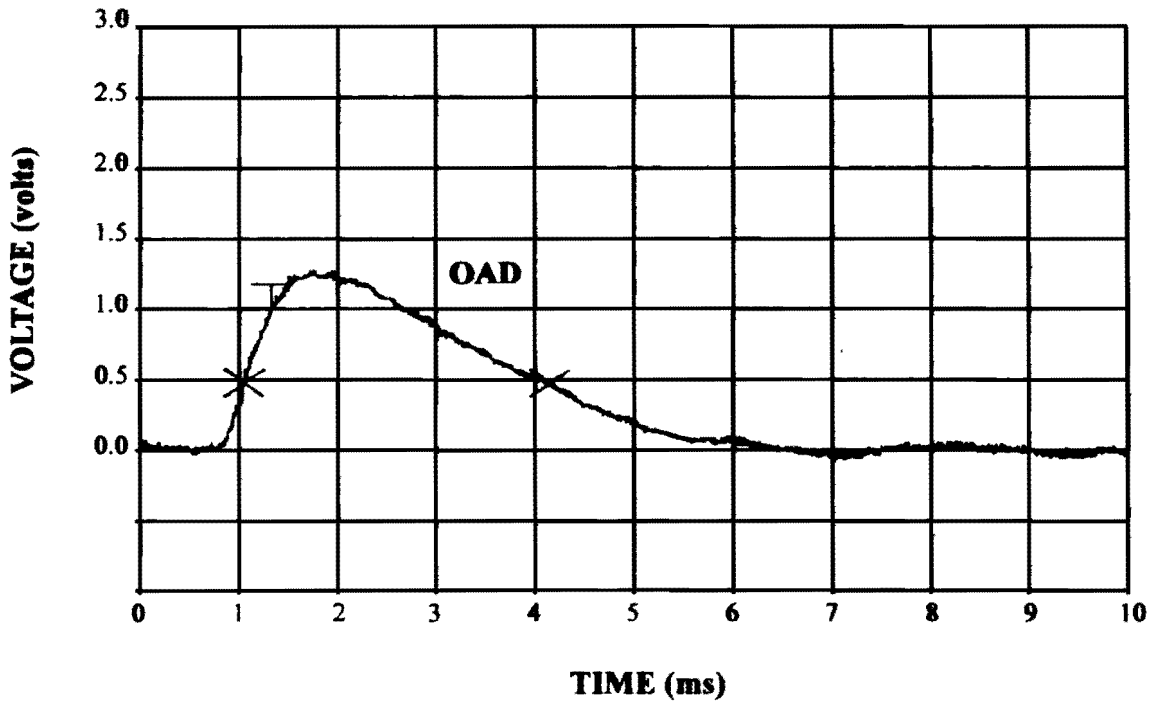


Figure 10. The demodulated signal of a 1.0 mm raindrop impact using the APL (top) and OAD (bottom) circuits.

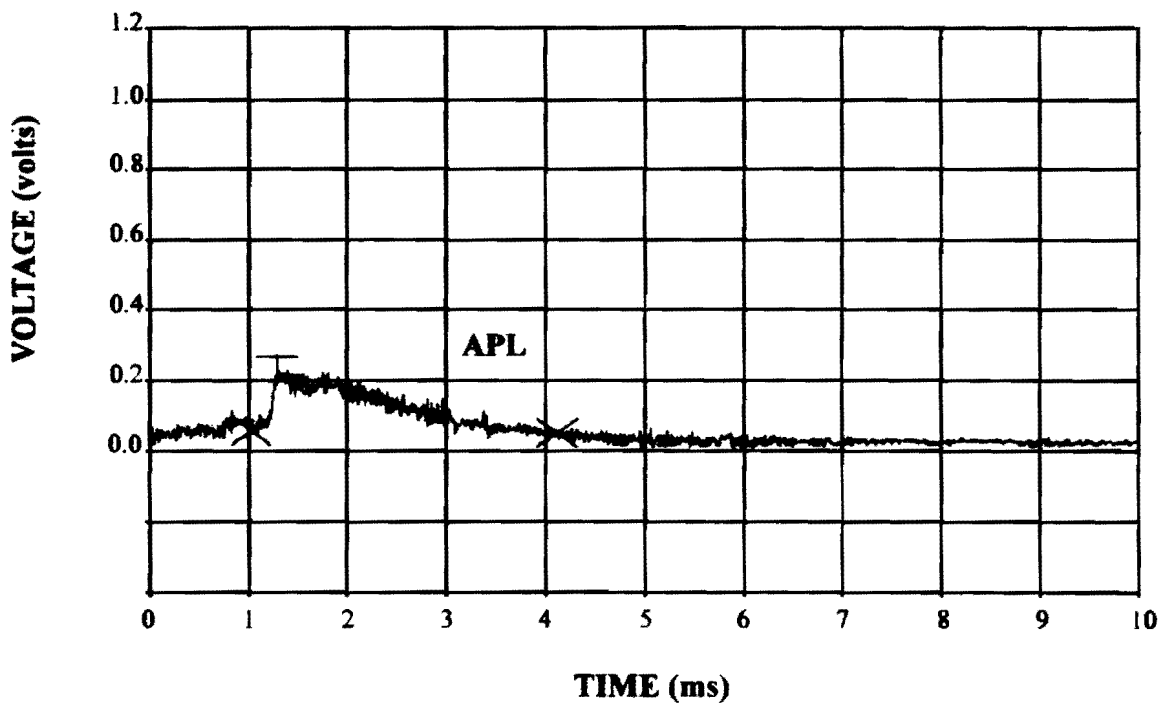
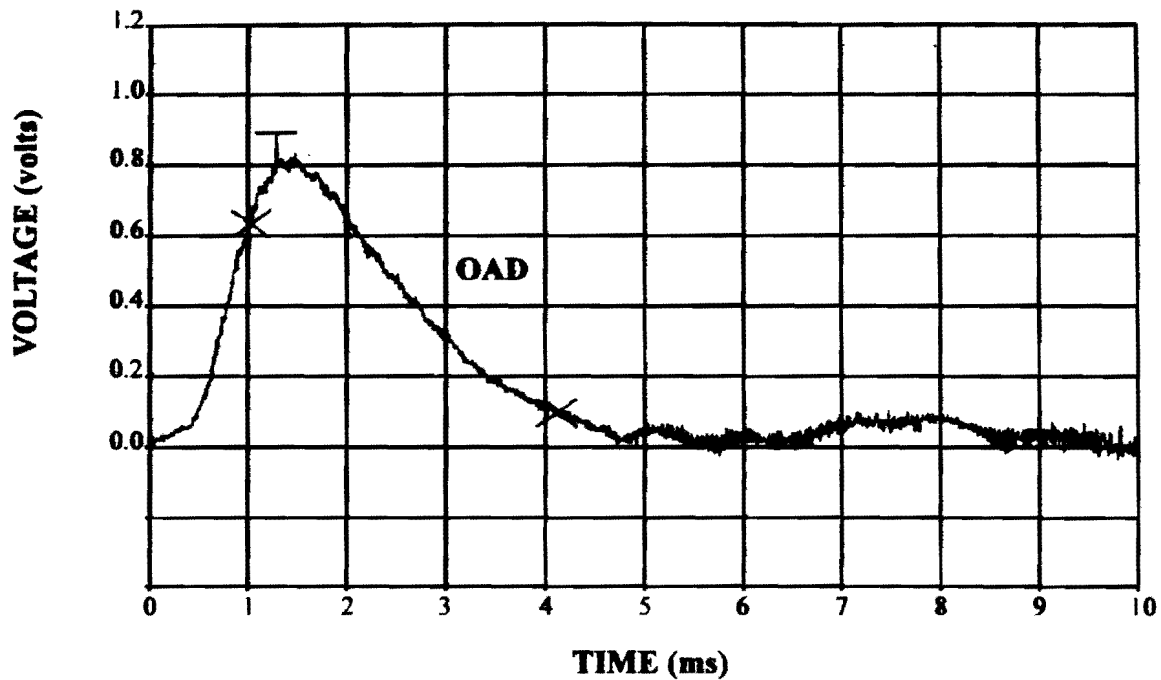


Figure 11. The demodulated signal of a 0.8 mm raindrop impact using the APL (top) and OAD (bottom) circuits.

## B. Temperature Sensitivity

Realistic operating temperatures range from 0-40°C, although an instrument exposed to sunlight may get hotter at times. The onset of rain will rapidly cool the sensor, requiring that temperature sensitivity be evaluated. The temperature sensitivity of the APL and OAD demodulator circuits were evaluated by placing the circuits in a temperature-controlled oven. Six temperatures between 11.1 and 69.9°C were used. After being allowed to come into temperature equilibrium for one hour, ten different input voltages (90 dB range) were applied to the circuit, and the output of each demodulator circuit was recorded.

The data are displayed in two formats. Figure 12 shows output voltage as a function of input voltage for the six temperatures used (11.1, 24.2, 35.7, 46.9, 57.7 and 69.9°C). An input voltage of 0 dB relative to 0.5 V is equivalent to the signal from a 5.5 mm raindrop. An input voltage of -70 dB relative to 0.5 V is equivalent to the signal from a 0.6 mm raindrop. Over this range (0 to -70 dB), the OAD circuit shows no temperature sensitivity, while the APL circuit shows some temperature sensitivity, especially between -70 and -30 dB. In Figure 13 the same output voltage data is shown as a function of temperature for different input voltages. Note that for the OAD circuit the field threshold for drop detection is set at approximately 0.2 V output voltage.

## C. Peak Detector

The original peak detector in the computer interface module, made by the Burr-Brown Corp., is no longer available. A substitute peak detector was designed by APL engineers. A commercially available, inexpensive peak detector built by Analog Devices was also tested. The stability and percentage error for each of these detectors was evaluated by applying a known input voltage and recording the output peak value. Table 1 shows the test results. The best peak detector is the Analog Devices (P/N PKD01EP) peak detector. It showed the highest accuracy. There are no time delays introduced. Furthermore, it is commercially available (the APL unit is a fabricated circuit board) and inexpensive (\$15). The Analog Devices peak detector should be a permanent component in the modified APL disdrometer computer interface circuit.

Table 1. Peak detector comparison values for the Burr-Brown (BB), Applied Physics Laboratory (APL), and Analog Devices (AD) peak detectors.

Voltage In	Peak Value Detected (V)			Percentage Error		
	BB	APL	AD	BB	APL	AD
0.503	0.498	0.537	0.500	0.79	6.97	0.60
1.003	0.999	1.033	1.001	0.39	3.09	0.20
1.503	1.499	1.526	1.501	0.27	1.59	0.13
2.003	1.997	2.026	2.000	0.29	1.15	0.15
2.503	2.498	2.534	2.500	0.19	1.24	0.12
3.003	2.998	3.052	3.000	0.17	1.63	0.10
3.503	3.496	3.594	3.501	0.19	2.59	0.06
4.003	3.997	4.158	3.999	0.15	3.87	0.10
4.503	4.495	4.734	4.500	0.18	5.49	0.07

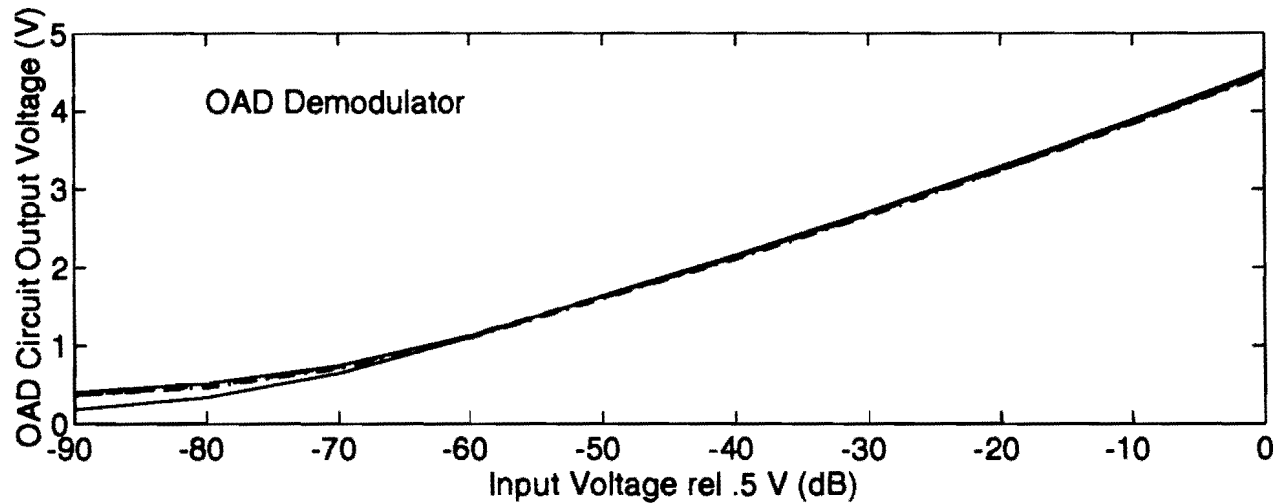
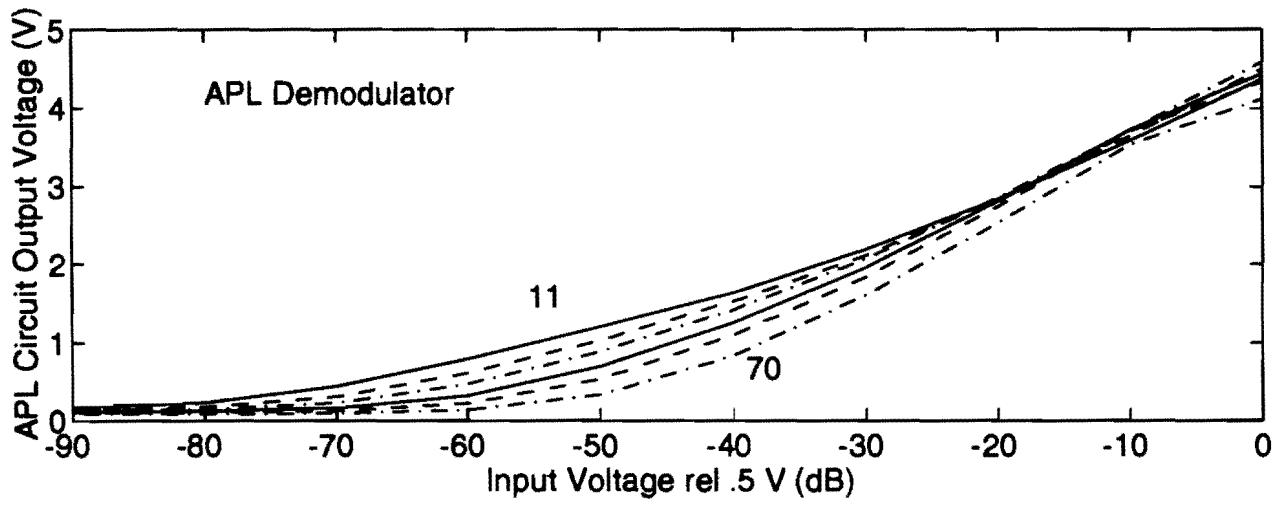


Figure 12. APL (top) and OAD (bottom) demodulator output voltage as a function of input voltage for different ambient temperatures. The different temperatures are 11, 24, 36, 47, 58 and 70°C.

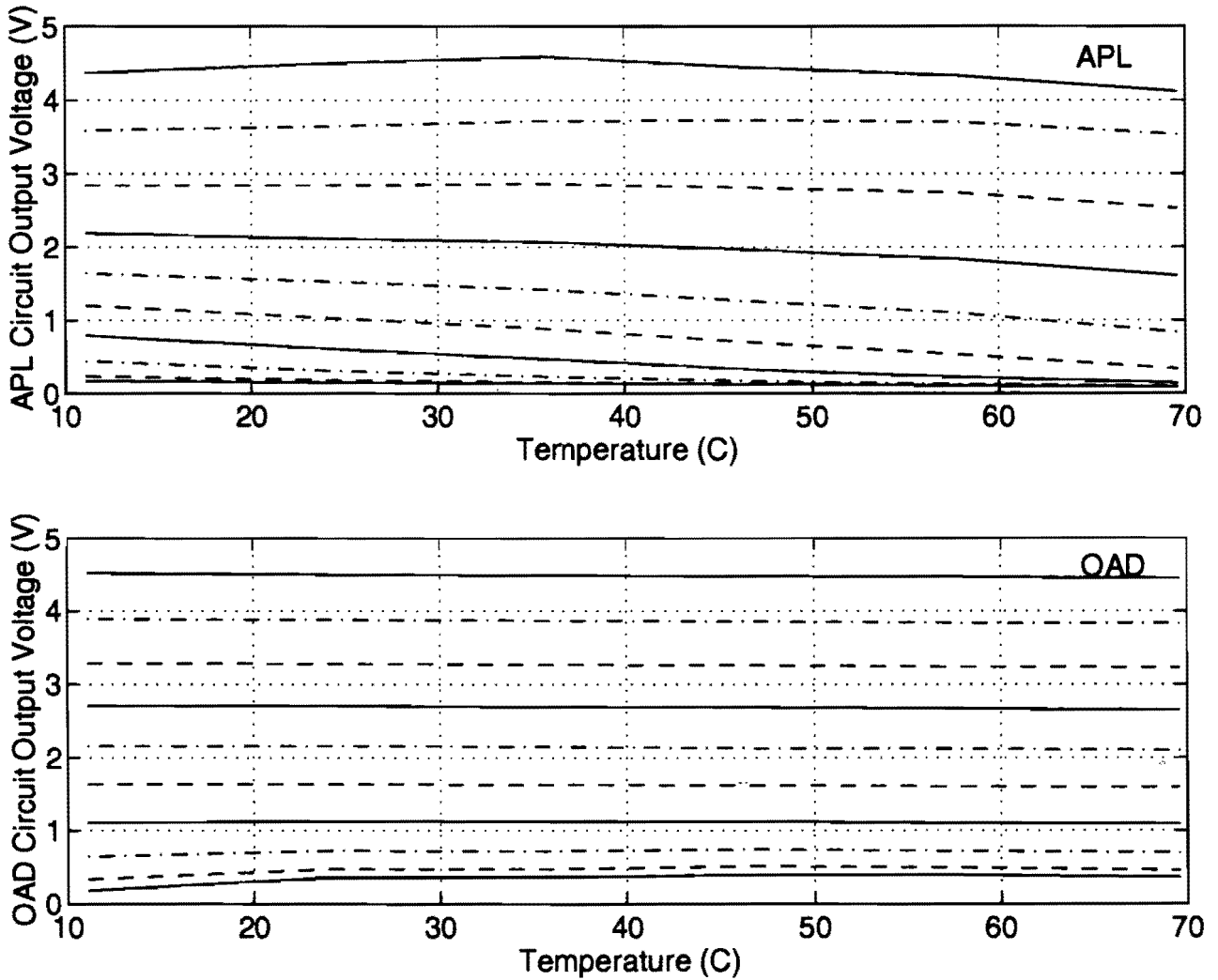


Figure 13. APL (top) and OAD (bottom) demodulator circuit output voltage as a function of ambient temperature for different input voltages. The input voltage ranges from 0 dB rel 0.5 V (top line) to -90 dB rel 0.5 V (bottom line) in 10 dB increments.

## 6. CALIBRATION

Calibration of the modified APL disdrometer system was performed using synthetic raindrops (0.6-5.5 mm diameter) striking the sensor head at terminal velocity. A relationship between drop size and peak voltage detected was obtained empirically. The "down time," the time interval between the time that the peak detector threshold level is exceeded and the time that the processing computer resets the peak detector, was also measured empirically for each drop size.

### A. Synthetic Raindrop Production

Generating realistic raindrops is important because the impact physics are affected by drop size, shape, and impact velocity. At terminal fall velocity, raindrops larger than 1 mm diameter are significantly deformed by air drag (Pruppacher and Pitter, 1971). Two problems must be addressed: How does one generate a full range of raindrop sizes (200  $\mu\text{m}$ -6 mm diameter) and how far must the drop fall to reach terminal velocity?

At OAD, two synthetic raindrop production apparatus were constructed (Figure 14). In both apparatus, a water reservoir is attached to a needle valve which controls the flow rate through different diameter copper tubing. For larger raindrop sizes (2.5-5.5 mm diameter), water was allowed to drip off the end of copper tubing of various inner diameters (0.2-5 mm). The relationship between tube diameter and drop size is shown in Figure 15. It was found that, as long as individual drops were allowed to form at the tube tip, the flow rate did not affect drop size. Drop sizes were determined by weighing 100 drops for each tube size in groups of 20 drops each. The mean weight and standard deviation for each tube size are shown in Table 2.

In order to generate smaller drop sizes, the individual drops must be actively knocked off of the tube tip. To accomplish this, the smallest diameter tubes were mounted onto an audio speaker which was driven by a sine wave of variable frequency. By varying the frequency of the sine wave driver, drop sizes from 0.6-2 mm diameter were created (Figure 16). The drop sizes were determined by collecting 15-20 individual drops on a water repellent surface and then measuring their diameter using precision calibrated optical magnifying lenses. The drop sizes were verified before each experimental run because the relationship between drop size and driver frequency was not stable.

Table 2. Synthetic drop production statistics.

Tube Diameter (mm)	Mean Weight (g)	Standard Deviation (g)	Mean Drop Diameter (mm)	Drop Size Range (mm)
0.20	.008	.00025	2.5	2.5
0.25	.010	.00025	2.7	2.7
0.41	.013	.00027	2.9	2.9
0.84	.024	.00300	3.6	3.4-3.7
1.60	.037	.00500	4.1	3.9-4.3
2.16	.048	.00650	4.5	4.3-4.7
3.00	.059	.00880	4.8	4.6-5.1
5.00	.084	.00800	5.5	5.3-5.6

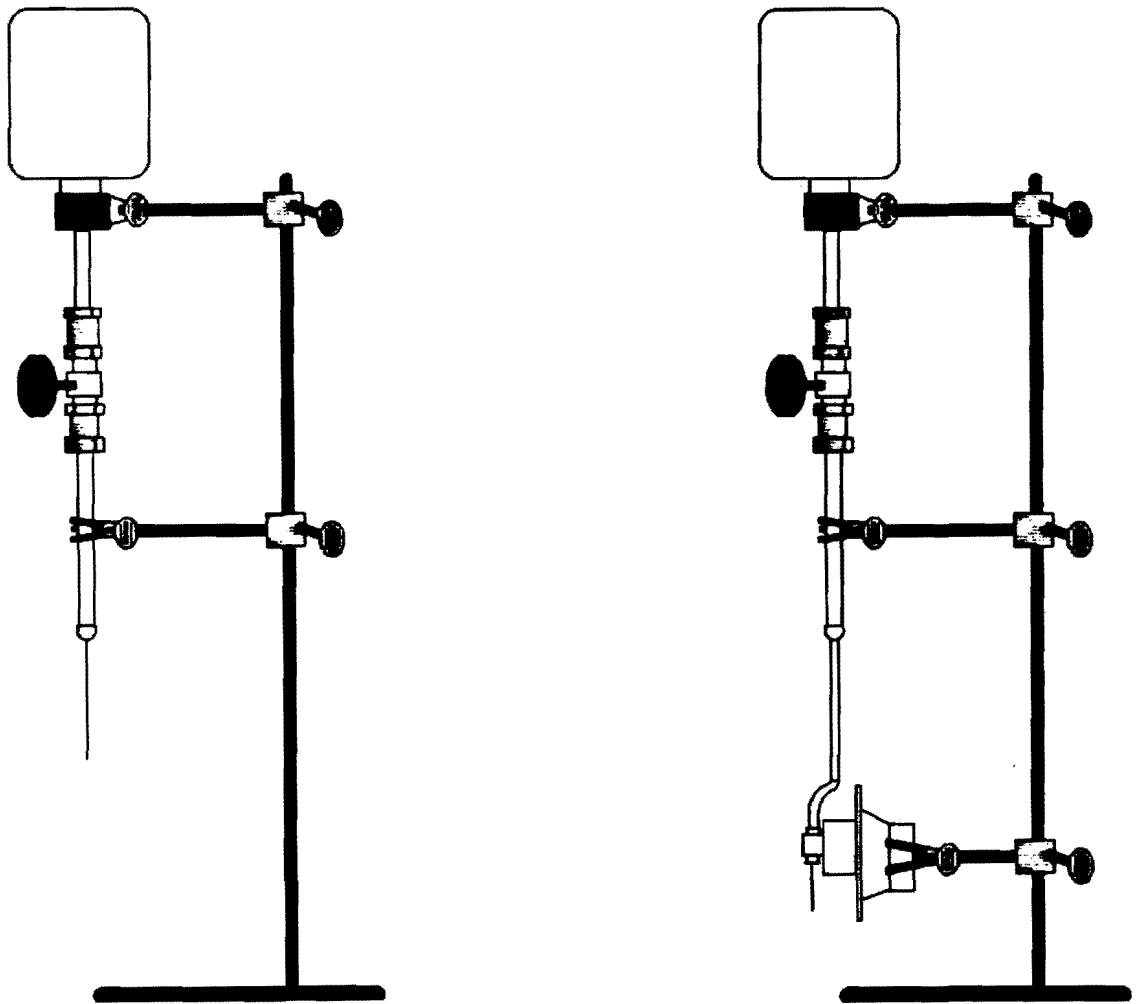


**Figure 14. Synthetic drop production apparatus. The large drop maker (left) generates different sized drops by allowing drops to form at the end of different diameter tubes. The small drop maker (right) actively knocks drops off the tip of a small tube using an audio speaker.**

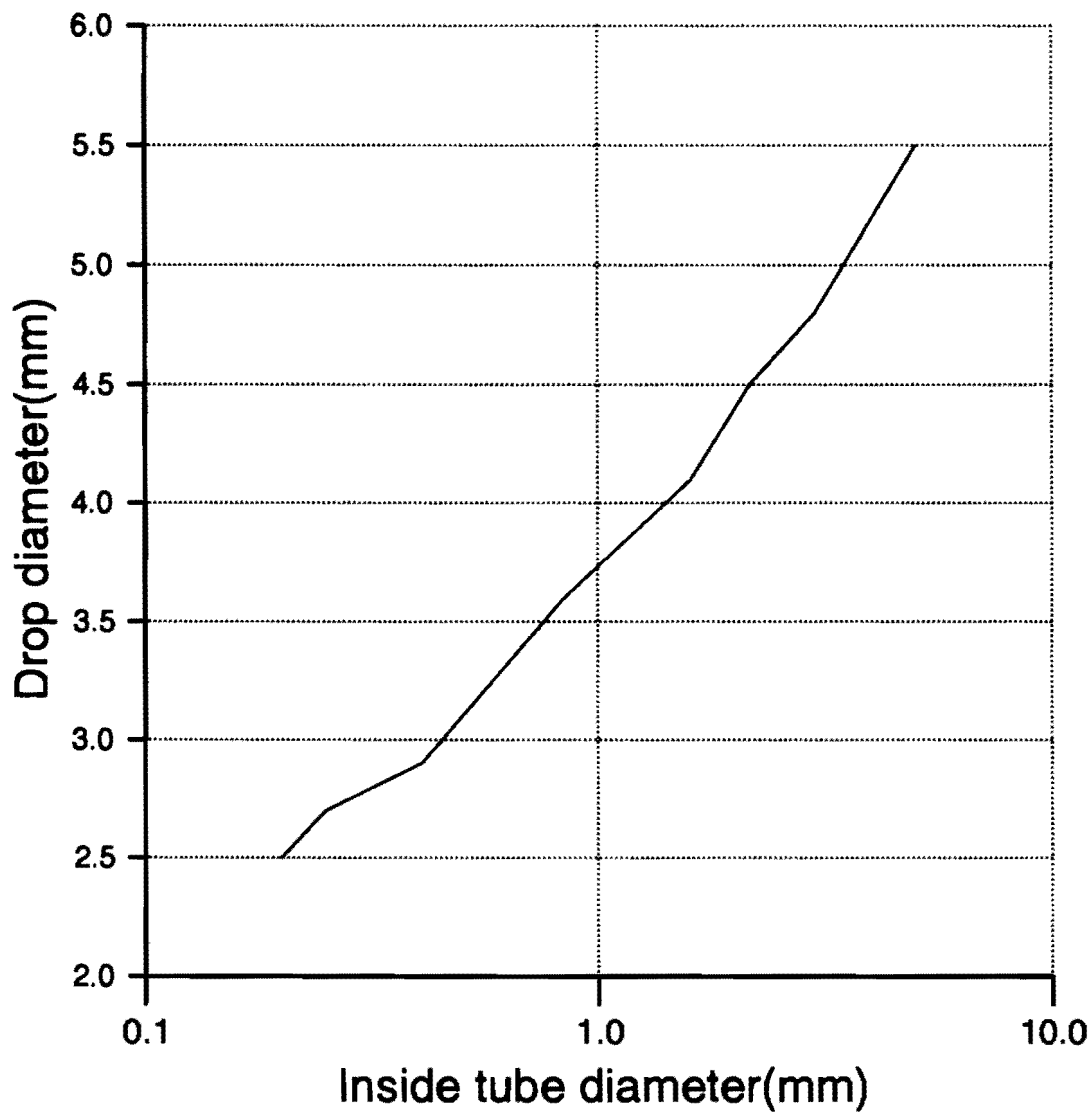


Figure 15. The relationship between tube size (inner diameter) and drop size (mm) using the large drop maker.

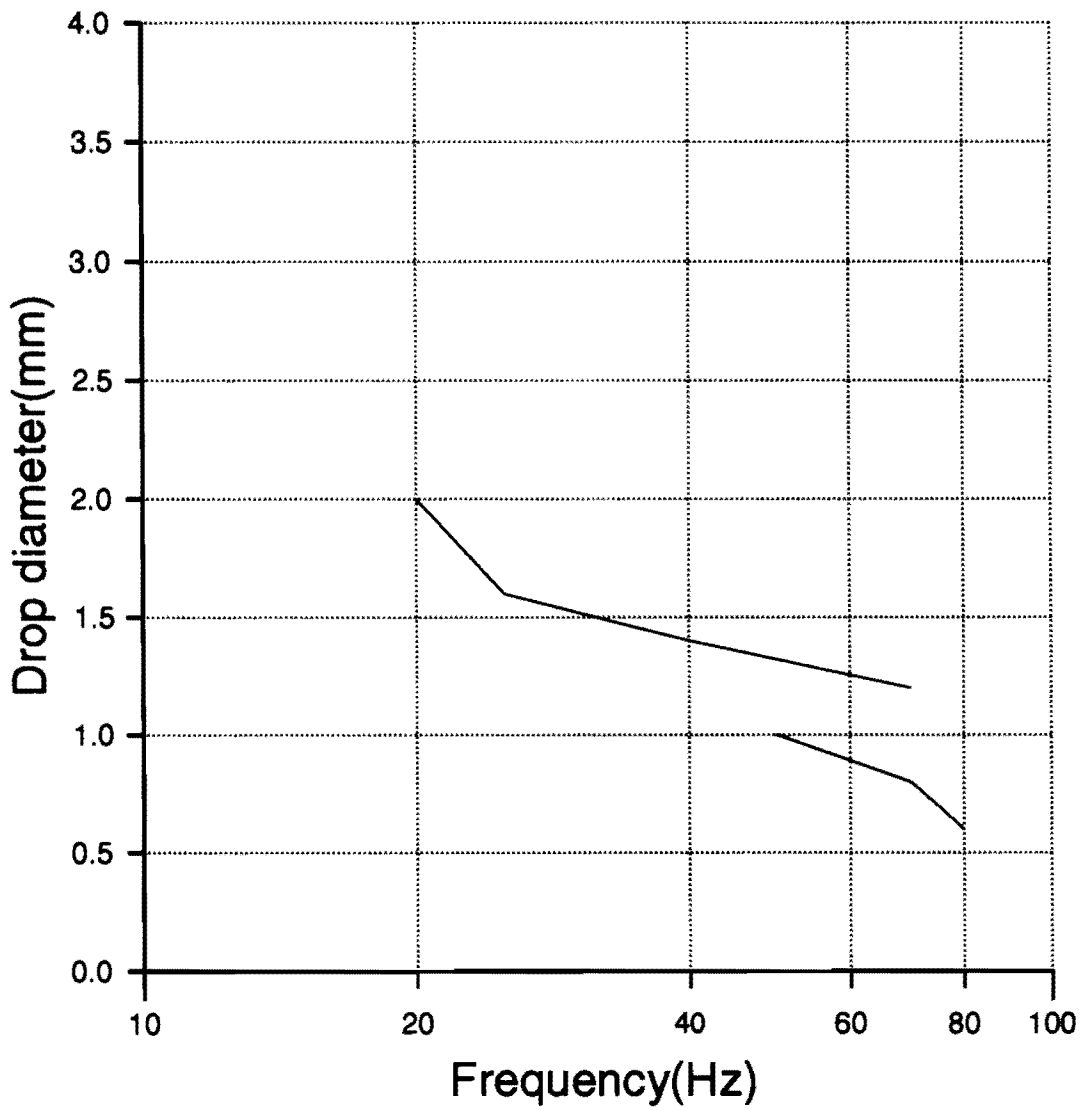


Figure 16. The relationship between audio speaker frequency and drop size (mm) using the small drop maker. The top curve is for a 0.3 mm inner diameter tube and the bottom curve is for a 0.2 mm inner diameter tube.

To obtain terminal impact velocity, drops were allowed to fall five stories in an internal stairwell. Wang and Pruppacher (1977) determined that a fall height of at least 12 m is required for the largest drop sizes to obtain terminal velocity. The stairwell met this requirement. For the small drop sizes, a shorter fall height (4.5 m) was used to assure that the drops hit the sensor surface; the small drops exhibited significant horizontal drift as they fell. For two of the small drop sizes generated (1.6 and 2 mm), the 4.5 m fall height was insufficient to obtain terminal velocity (Wang and Pruppacher, 1977). Calibration data for these two drop sizes were adjusted to an equivalent raindrop size at terminal velocity using equivalent drop momentum (Figure 2).

## B. Calibration Procedure

Drop collection was automated. Peak voltage for approximately 100 drop impacts for each of 15 drop sizes ranging from 0.6-5.5 mm diameter were collected. Spurious data points (low voltage values) due to drop breakup, near misses, spatter, and noise were removed subjectively. The remaining data were evaluated for mean, mode, and median voltage values. Figures 17 and 18 show the resulting calibration curve using the mean and mode of the data. The curves are proportional to drop momentum (Figure 2), indicating that this is the physical quantity being measured by the sensor element. The first order least square (logarithmic) relationship using the mean of the calibration data is

$$\text{Diam} = 10^{(.2576 \cdot V - .3747)}$$

where Diam is the drop diameter (mm) and  $V$  is the peak voltage (V).

Figure 19 shows that the time interval during which the demodulated pulse is greater than a 0.6 V detection threshold is a function of drop size. During this time interval, additional drops striking the sensor will not be detected, although if the new drop is larger than the original drop, the peak voltage value will be for the new drop. If a smaller drop strikes, it will be undetected. In either case, the time interval that the threshold is exceeded will be longer than a strike by a single raindrop; the sensor head will be re-excited by the additional drop impacts and take longer to decay back to below the threshold level.

## 7. FIELD TESTS

Field tests using the modified APL disdrometer were conducted at the AOML Rain Gauge Facility (Figure 20). A Joss-Waldvogel disdrometer and a weighing rain gauge were co-located with the APL disdrometer. The chronology of the field deployments of the APL disdrometer is shown in Table 3. Overall rainfall rate and drop counts within selected size intervals were compared over six rain events.

### A. Joss-Waldvogel Disdrometer Data

The Joss-Waldvogel RD-69 disdrometer (Joss and Waldvogel, 1969) system consists of a sensor head and a RD-69 processing box. The sensor head has a surface area of 50 cm<sup>2</sup>. A pulse from an impacting raindrop is filtered and converted into an electrical pulse by the RD-69 processing box. This pulse is sent to an analog-digital interface unit, the ADA-90. The signal is converted to drop size using a manufacturer supplied algorithm. These data are binned into 20 drop size categories and are stored into a dedicated processing computer once per minute. An example of Joss-Waldvogel disdrometer data is shown in Figure 21. Note the suppression of the smallest three drop size categories during the heaviest portion of the rain (from minutes 8-20 the rainfall rate exceeded 100 mm/hr). This variable background threshold level is built into the processing electronics (RD-69 box).

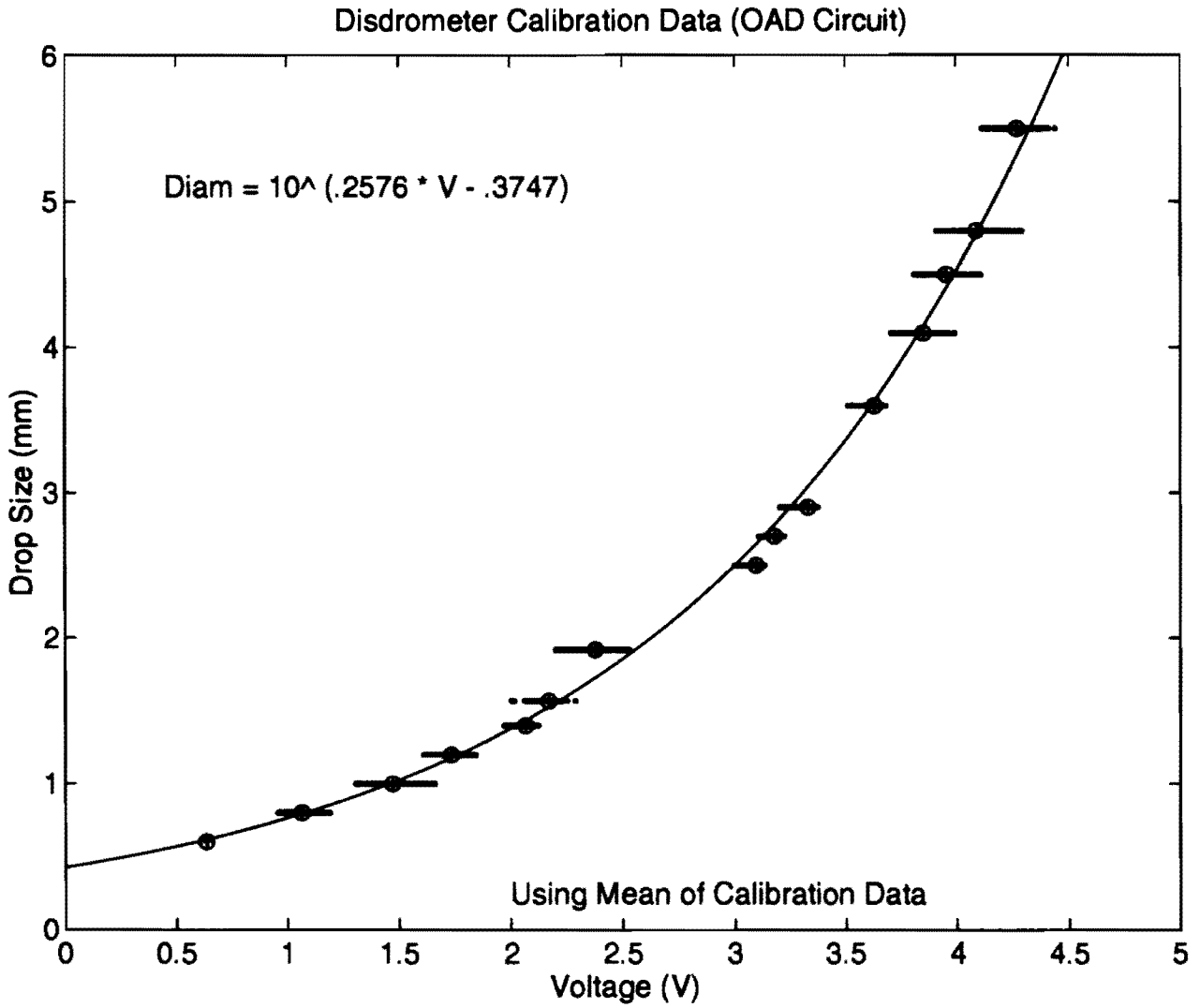


Figure 17. APL disdrometer calibration curve using mean drop size.

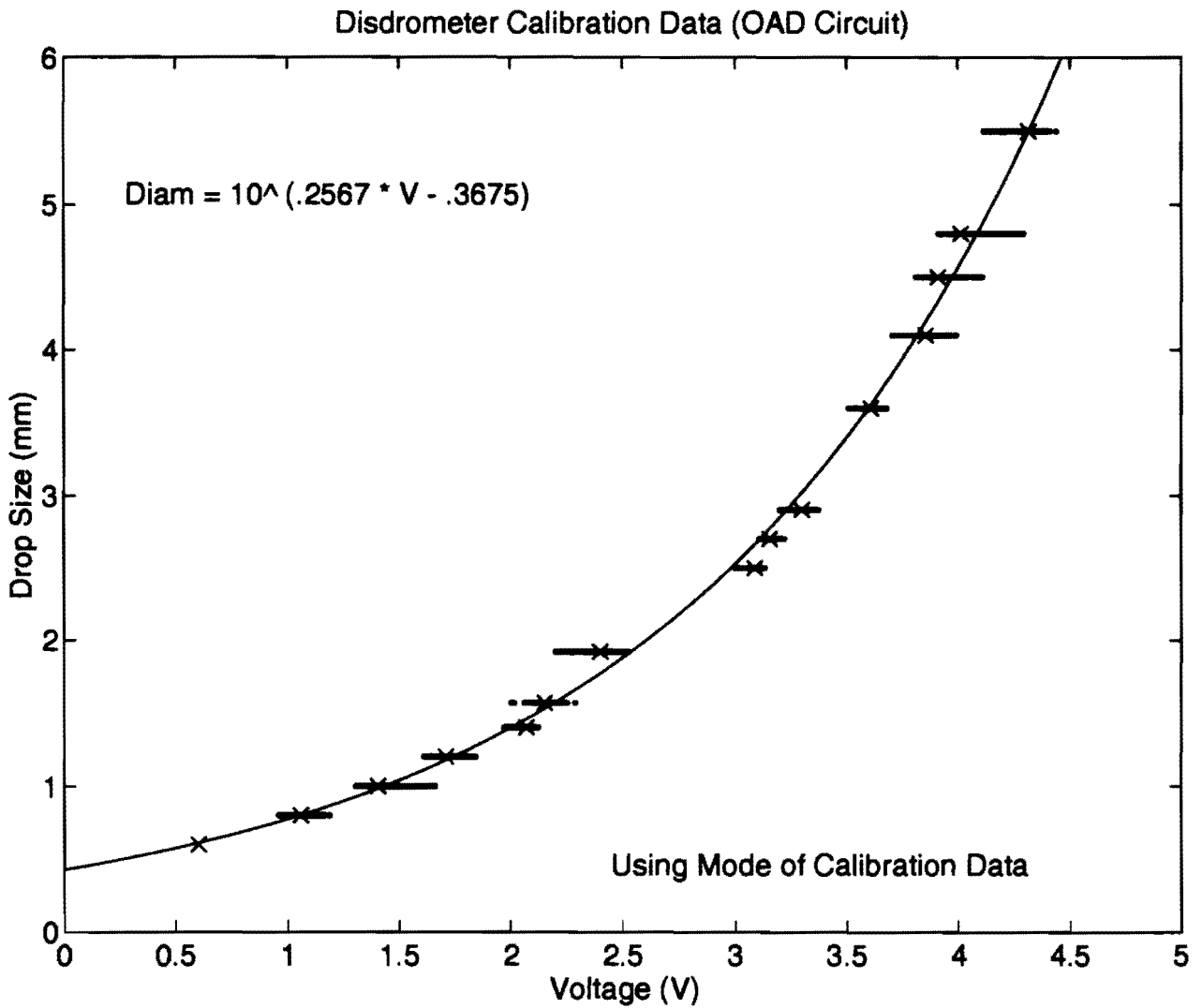


Figure 18. APL disdrometer calibration curve using drop size mode data.

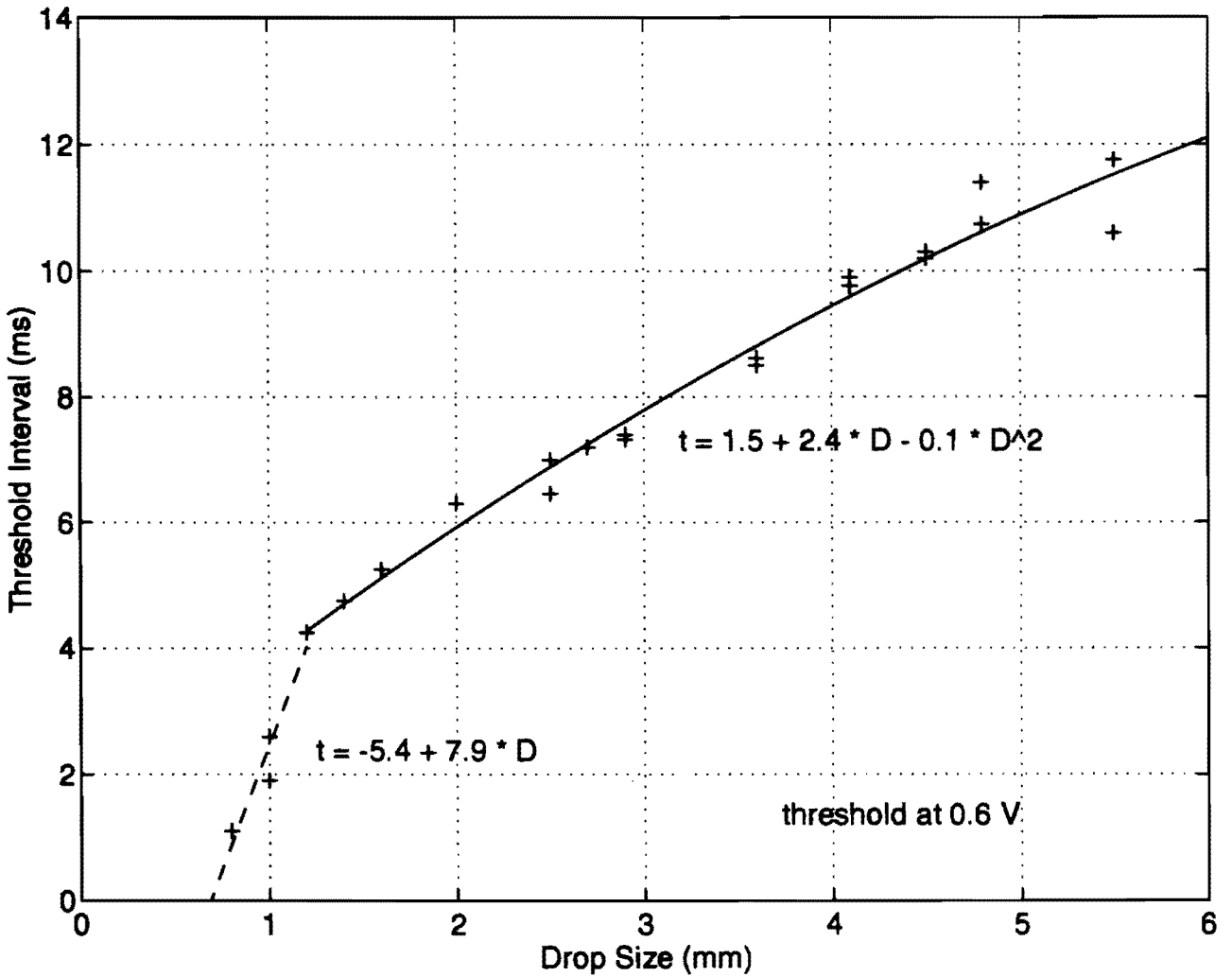


Figure 19. APL disdrometer down time as a function of drop size. This is the time interval that the demodulated signal is above a threshold of 0.5 V. During this time, additional drops will not be counted (but may affect the signal amplitude).

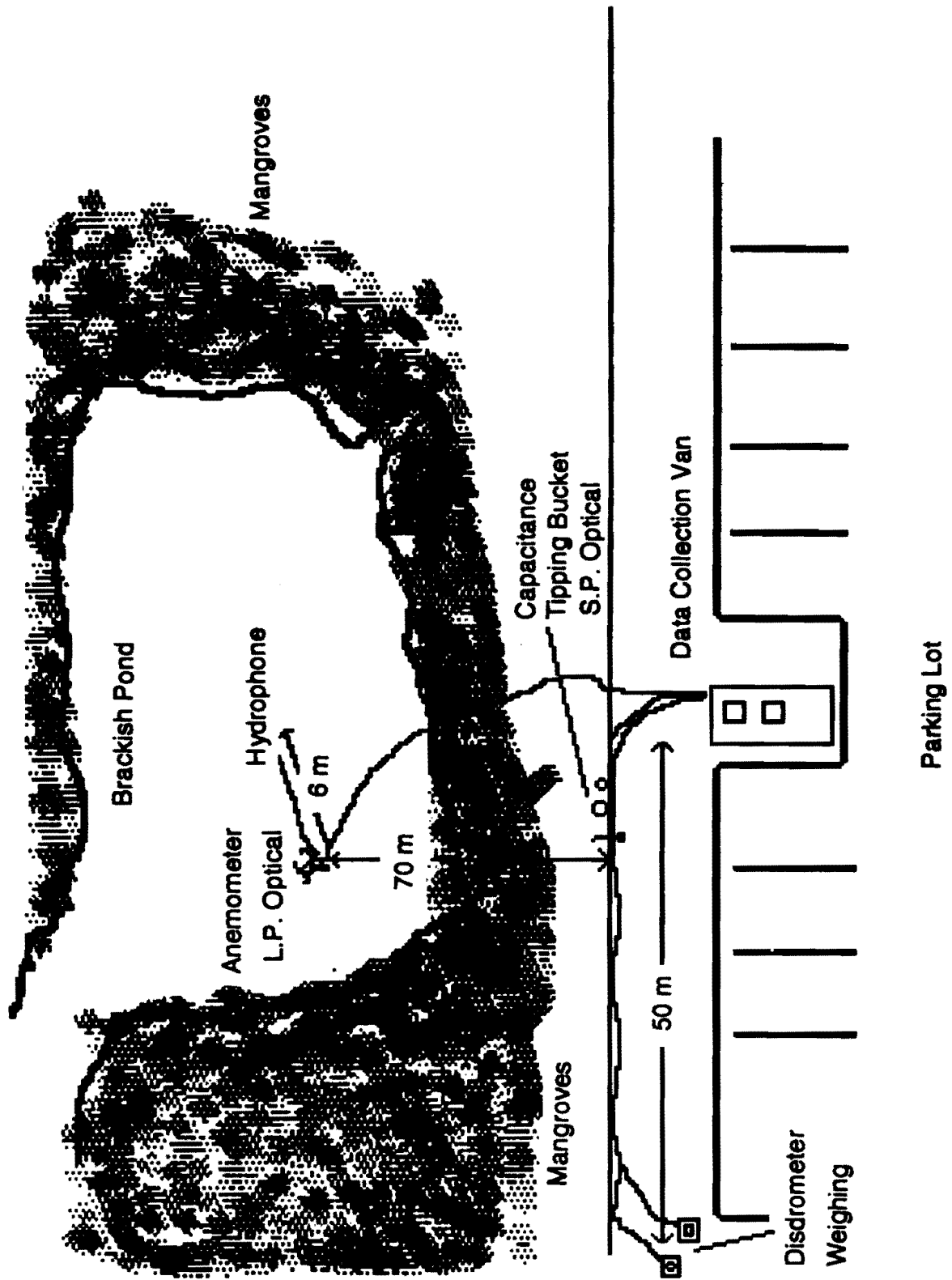


Figure 20. The AOML Rain Gauge Facility.

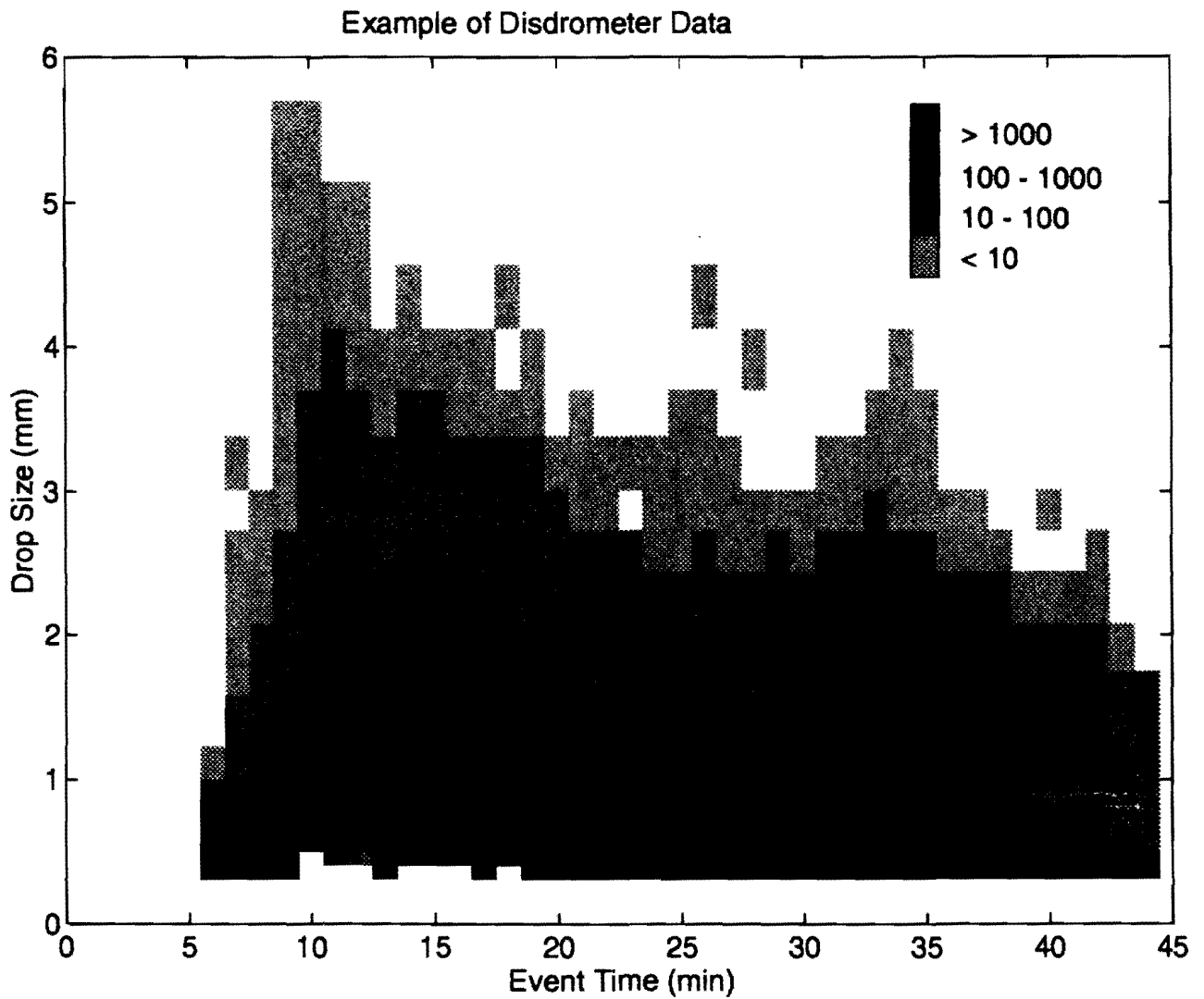


Figure 21. An example of Joss-Waldvogel disdrometer data.

Table 3. APL disdrometer evaluation chronology.

Julian Day	Date	Action
108	4/19/94	APL disdrometer deployed.
114	4/24/94	Field data collected.
115	4/25/94	Burr-Brown peak detector replaced by APL circuit.
122	5/02/94	APL and Joss-Waldvogel disdrometers removed for inspection (problem with sensor head).
126	5/06/94	APL and Joss-Waldvogel disdrometers returned to field. Clamping circuit installed in APL.
136	5/16/94	Both disdrometers removed for lab tests.
139	5/19/94	Calibration drop data (four sizes) collected using both disdrometers.
139	5/19/94	Both disdrometers returned to field. APL disdrometer has new sensor head.
145	5/25/94	Field data collected.
149	5/29/94	Field data collected.
150	5/29/94	Field data collected.
160	6/09/94	Both disdrometers removed for calibration.
161	6/10/94	Large drop calibration data collected (eight sizes) using both disdrometers.
161	6/10/94	Both disdrometers returned to field.
161	6/10/94	Field data collected.
168	6/17/94	Both disdrometers removed for calibration.
173	6/22/94	Small drop calibration data collected (seven sizes) using both disdrometers.
175	6/24/94	Both disdrometers returned to field.
181	6/30/94	Clamping circuit in APL disdrometer removed. New C processing program installed and running (delay times reduced).
191	7/10/94	Field data collected.
193	7/12/94	APL disdrometer removed for service.
194	7/13/94	Smoothing filter added to APL disdrometer.
196	7/15/94	APL disdrometer returned to field.
199	7/18/94	Both disdrometers removed for calibration.
202	7/22/94	Calibration data collected (all drop sizes; both disdrometers).
203	7/22/94	Both disdrometers returned to field.
204	7/23/94	Field data collected.
205	7/24/94	Field data collected.
206	7/25/94	Field data collected.
210	7/29/94	Field data collected.
220	8/08/94	APL disdrometer removed from field.
221	8/09/94	APL disdrometer and OAD circuits compared using eight large drop sizes.
222	8/10/94	APL disdrometer and OAD circuits compared using two small drop sizes.
223	8/11/94	APL disdrometer returned to field.

High small drop counts were also observed at the beginning of the storm and, then, later from minutes 30-50. Maximums in drop size distribution are rarely observed for such small drop sizes. At the beginning of a convective storm, scattered very large raindrops occur. These drops fall much faster than other drop sizes and, therefore, reach the ground first. Very small drops should not be present. Later, stratiform drizzle is falling. Drop coalescence and scavenging usually removes the very small drops from the rain. The detected very small drops may be secondary splashes or incomplete noise suppression.

Because of the variable threshold and the unusual high drop counts in bins 1-4, data from these bins should be considered suspect. These drops are very small (0.3-0.7 mm diameter) and rarely comprise a significant fraction of water volume within the rain. Consequently, neglecting these drops does not severely bias overall rainfall rate estimates.

When a drop is detected, there is "down time" when the system can not detect an additional impacting raindrop. This down time interval is described as "very short" but is not explicitly incorporated into the data processing. The electrical pulse length is shown to be 0.5 ms in the manuals. This time interval is smaller than the APL circuitry by an order of magnitude, indicating that the correction factor to adjust for down time should be relatively small for the Joss-Waldvogel disdrometer. On the other hand, data (to be shown) suggests that the Joss-Waldvogel disdrometer underestimates extremely heavy rainfall rates (over 100 mm/hr), suggesting that a down time correction is an issue to be addressed.

## B. APL Disdrometer Data Processing

The APL disdrometer system consists of a sensor head, a demodulator unit, a computer interface unit, and a computer. The pulse of an impacting raindrop is demodulated, its peak level is detected, and data is transferred to the computer. Software, described in Appendix A, within the computer uses the calibration curve (Figure 17) to convert the voltage value to drop size. These drop size data can be tabulated to estimate drop size distribution in many different ways. To facilitate comparison to the Joss-Waldvogel data, the software was written to match the 20 drop size categories and the one-minute time interval of the Joss-Waldvogel disdrometer. In future applications, more drop size categories and smaller time intervals can be used. Note that drop size distributions are usually exponential in nature and so collecting a statistically significant number of large and very large drops in a short time interval is an issue.

There is a "down time" associated with each drop detection. During the time interval that the drop signal exceeds the peak detection threshold (Figure 19), no new drops can be detected. In addition, there is a 1.7 ms down time associated with the pulse processing software (time interval to accept the detection flag, digitize the peak value, bin and store the data, and release the detection flag). Finally, there is a down time associated with subsequent drops striking the sensor head during the threshold time interval of a previously detected raindrop. This is because the new drop will re-excite the sensor head, extending the time to drop below the detection threshold. Thus, the total down time for a data collection period (nominally one minute) is given by

$$\text{down time} = \sum_{i=1}^n N_i \tau_i + (1.7 \text{ ms}) \cdot \sum_{i=1}^n N_i + \left( \sum_{i=1}^n N_i \right) \cdot (1 - \text{duty cycle}) \cdot \tau_m / 2,$$

where  $N_i$  is the number of drops in the  $i$ th size bin during a data collection period  $T$  and  $\tau_i$  is the threshold time interval for a drop in the  $i$ th size category. The extended threshold time is estimated by the total number of drops detected in the data collection period times the probability of having a drop strike during the down time (1-duty cycle) multiplied by the average time that the threshold time would be extended (0.5 times the mean threshold time,  $\tau_m$ ). The duty cycle is given by

$$\text{duty cycle} = 1 - \text{down time}/T.$$

Recorded data must be adjusted to account for this duty cycle correction. Figure 22 shows the duty cycle during a heavy rainfall event. Figure 23 shows the total rainfall for this event before and after the correction factor is applied.

The APL demodulator produces shorter threshold time intervals than the OAD demodulator (by roughly 30%). While this feature of the APL demodulator would reduce the amplitude of the correction, a correction is still required. For example, during event 149 (Figure 22) the minimum duty cycle using the APL demodulator would be 0.75 rather than 0.69; an improvement, but not so large that the issue of duty cycle can be ignored.

For very high rainfall rates, it is important to include the correction for extended threshold times. At a very high rainfall rate, *e.g.*, 100 mm/hr, the average number of raindrops striking the sensor can exceed 50 per second, *i.e.*, the mean interval between drops is 20 ms. The mean threshold time for all raindrops is approximately 3 ms, suggesting that multiple drop arrivals are common during extremely heavy rainfall. Note that while Figure 19 shows threshold time intervals generally longer than 3 ms, the drop size distribution is generally numerically dominated by drops smaller than 1 mm diameter. The value of  $\tau_m = 3$  ms is based on observations over several different heavy rain events.

Finally, large numbers of multiple drop arrivals will bias the recorded distribution towards larger drop sizes. During the (extended) threshold time interval associated with multiple drop arrivals, only the peak voltage value (belonging to the largest drop) is detected. Only one drop is detected, the largest drop; the smaller drop merely extends the threshold time interval.

### C. Data Comparison

Figures 24-26 show estimates of rainfall rate from the APL disdrometer, the Joss-Waldvogel disdrometer, and the precision weighing rain gauge during three different rain events at the AOML Rain Gauge Facility. Overall the agreement is very good, although at very high rainfall rates the disdrometers underestimate the rainfall rate compared to the weighing rain gauge. The weighing rain gauge was in agreement with other types of automatic rain gauges within the AOML Rain Gauge Facility and can be considered a standard (Nystuen *et al.*, 1995). During the extremely heavy rain, the APL disdrometer rainfall rate estimate is closer to the weighing rain gauge value than the Joss-Waldvogel disdrometer. While this suggests that the APL disdrometer duty cycle correction is not complete, it also indicates that users of the Joss-Waldvogel disdrometer need to address this issue. The Joss-Waldvogel disdrometer manual has no discussion on duty cycle.

Within drop size categories, the APL and Joss-Waldvogel disdrometers are also in very good agreement (Figures 27-29). The drop size categories shown are: small, bins 5-7, 0.7-1.2 mm diameter; medium, bins 8-12, 1.2-2.4 mm diameter; large, bins 13-17, 2.4-4.1 mm; and very large, bins 18-20, >4.1 mm. Disagreement between the sensors appears to be random.

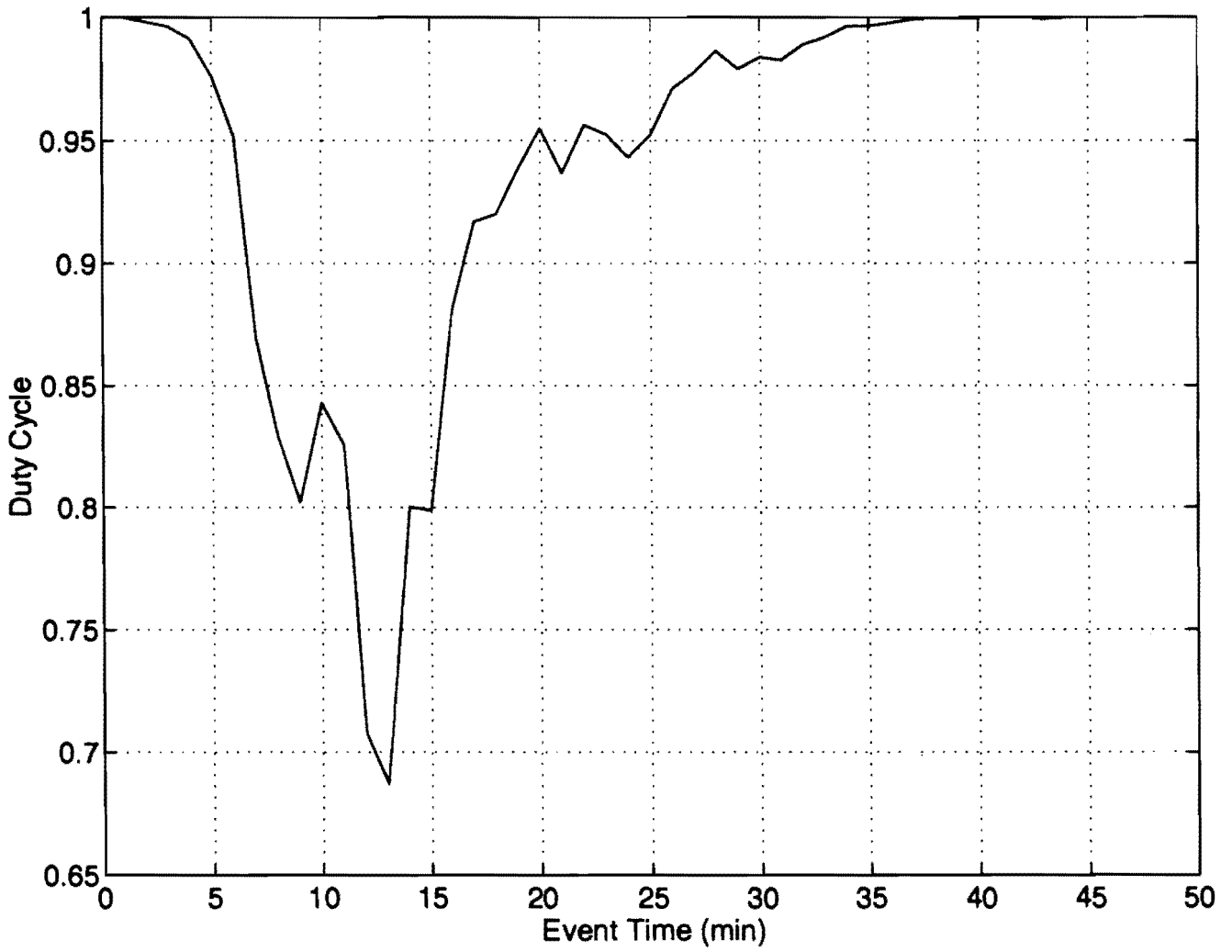


Figure 22. The duty cycle for the APL disdrometer during a heavy rainfall event on Julian Day 149 (1994).

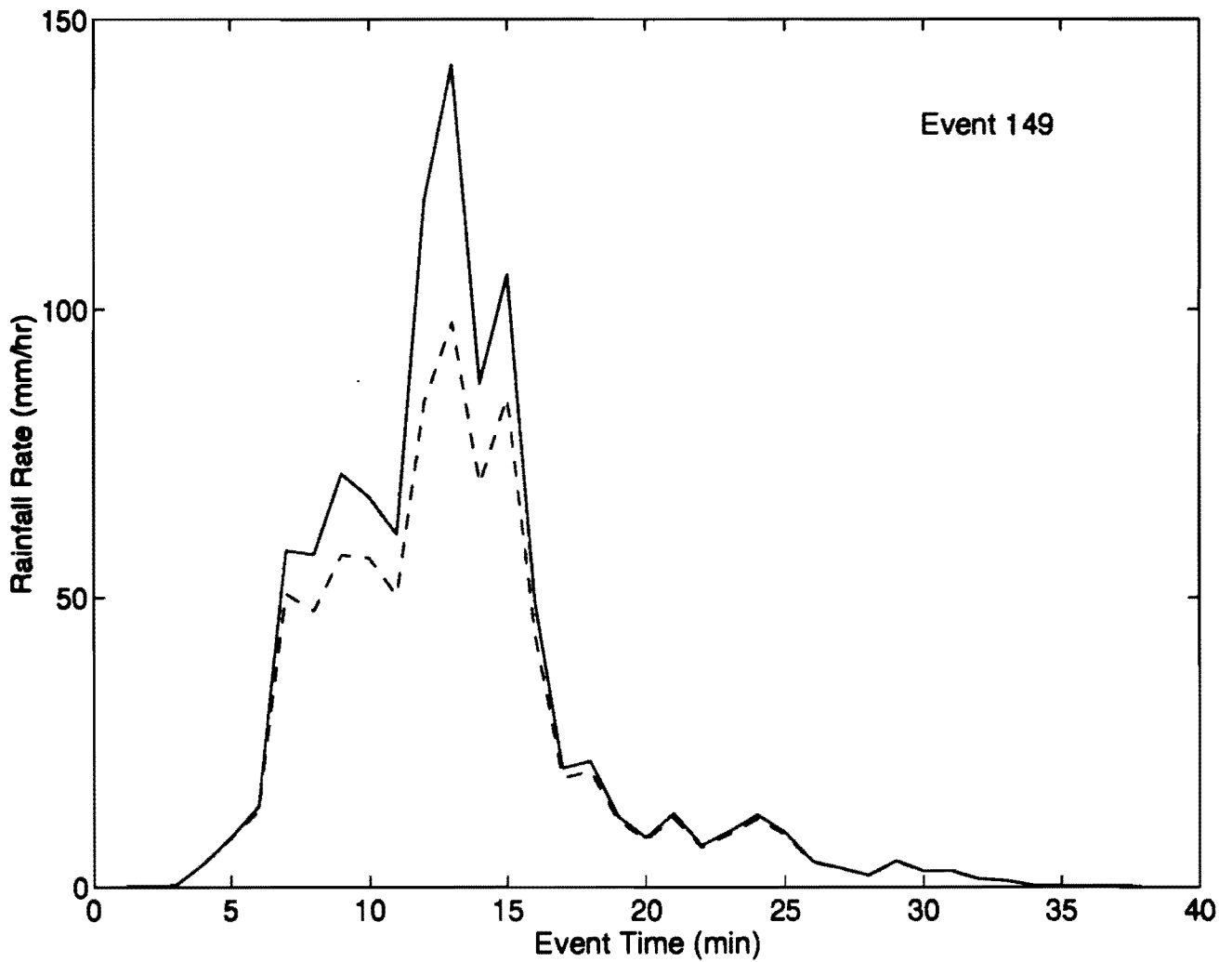


Figure 23. Total rainfall rate estimates before and after the duty cycle correction factor is applied.

Event 149 @ 2137 - Total Rainfall Rate

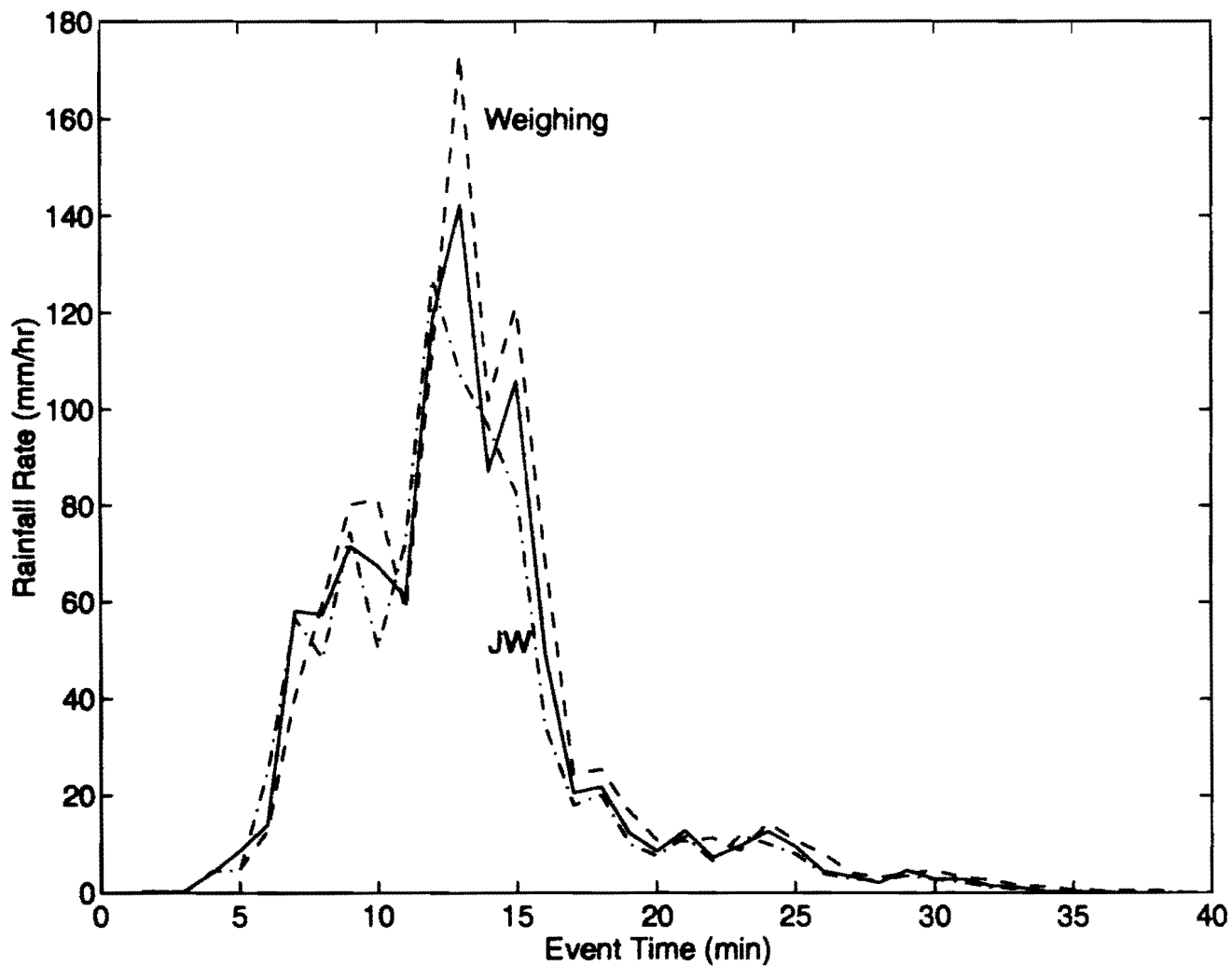
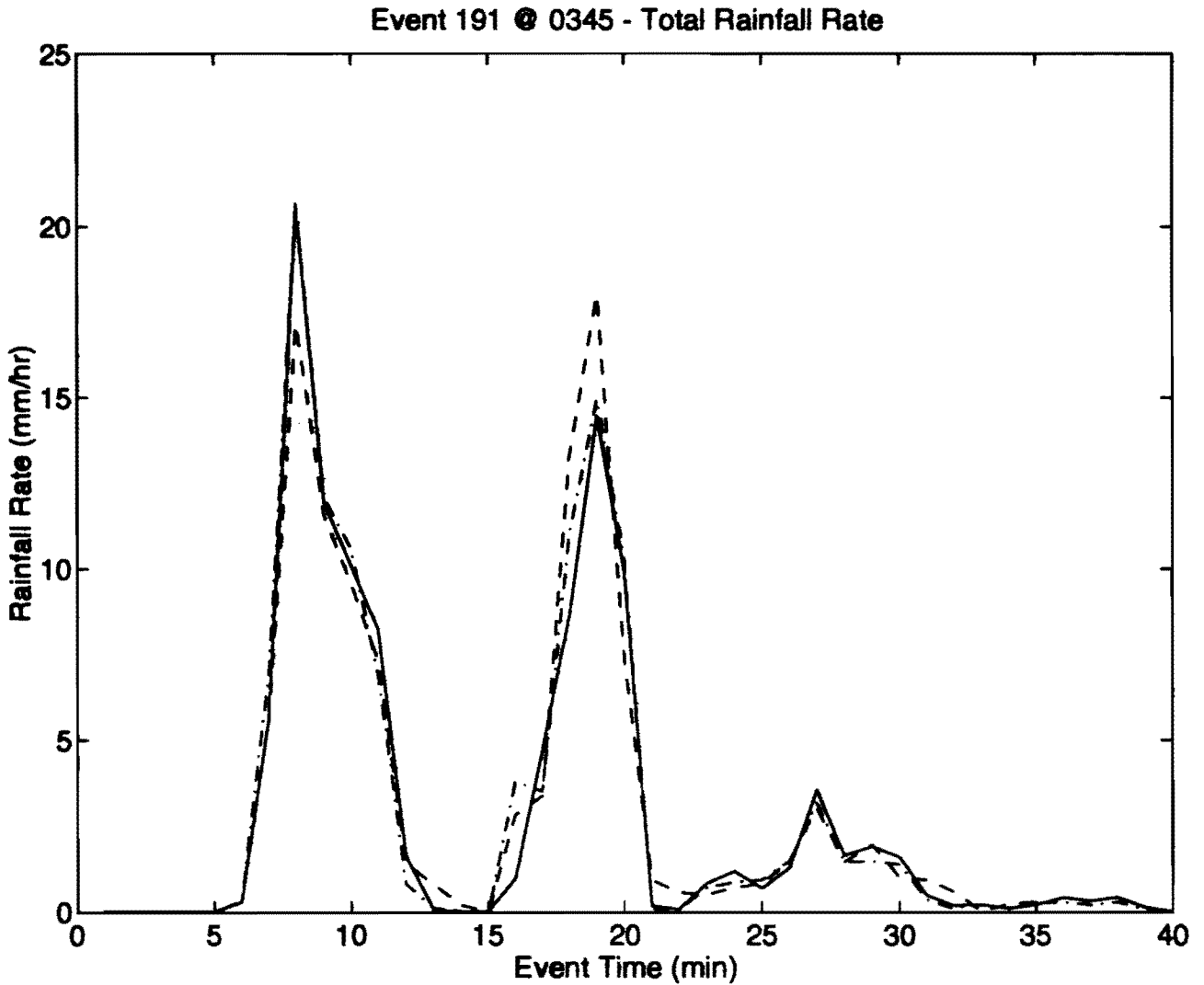


Figure 24. Total rainfall rate estimates for the APL (solid line) disdrometer, Joss-Waldvogel (dash-dot line) disdrometer, and a weighing rain gauge (dashed line) for a rain event on Julian Day 149 (May 29).



**Figure 25.** Total rainfall rate estimates for the APL (solid line) disdrometer, Joss-Waldvogel (dashed line) disdrometer, and a weighing rain gauge (dashed line) for a rain event on Julian Day 191 (July 10).

Event 210 @ 0907 - Total Rainfall Rate

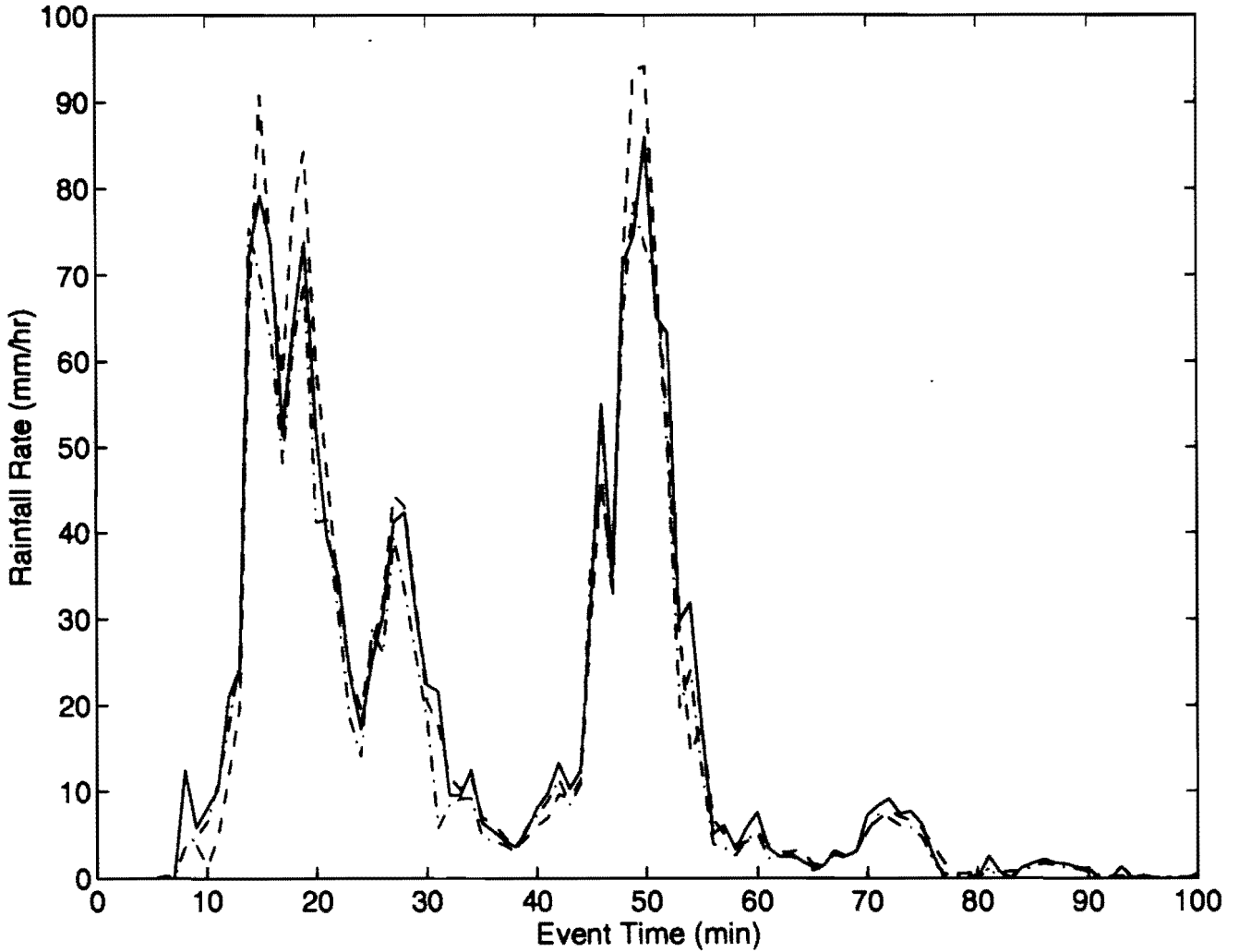


Figure 26. Total rainfall rate estimates for the APL (solid line) disdrometer, Joss-Waldvogel (dashed line) disdrometer, and a weighing rain gauge (dashed line) for a rain event on Julian Day 210 (July 29).

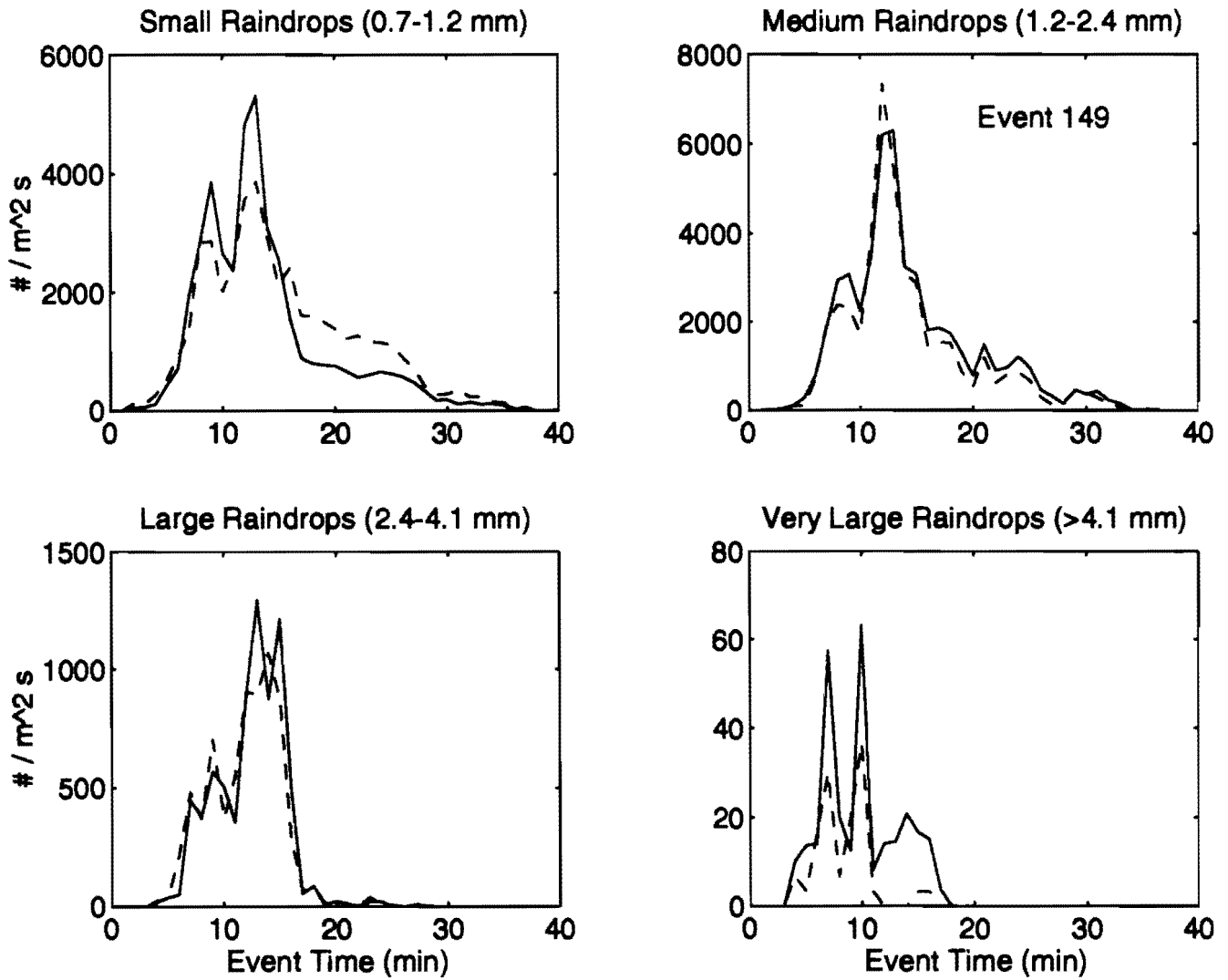


Figure 27. Comparison of drop size category (small, medium, large, and very large) counts for the APL (solid line) and Joss-Waldvogel (dashed line) disdrometers for the rain event of Julian Day 149 (May 29).

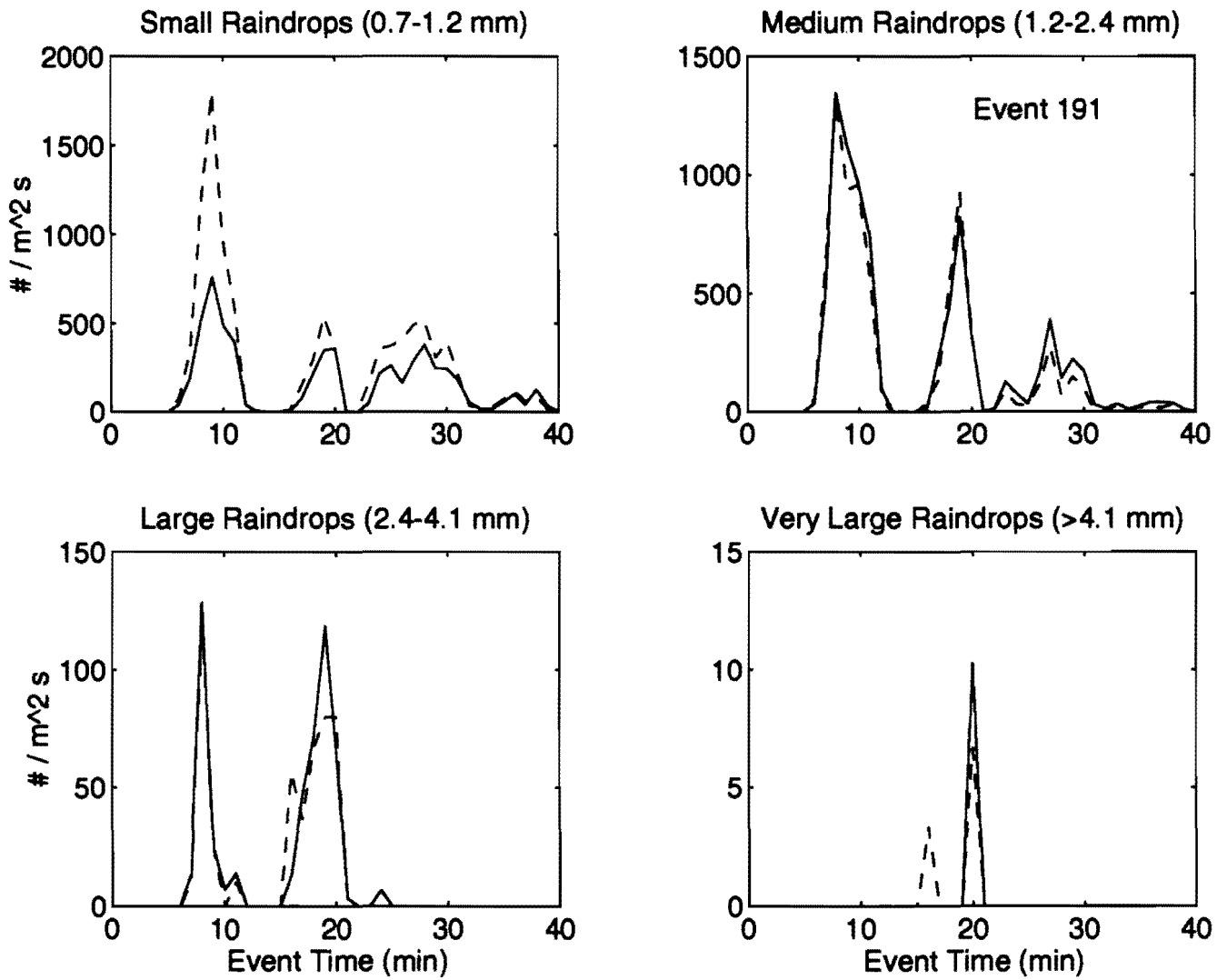


Figure 28. Comparison of drop size category (small, medium, large, and very large) counts for the APL (solid line) and Joss-Waldvogel (dashed line) disdrometers for the rain event of Julian Day 191 (July 10).

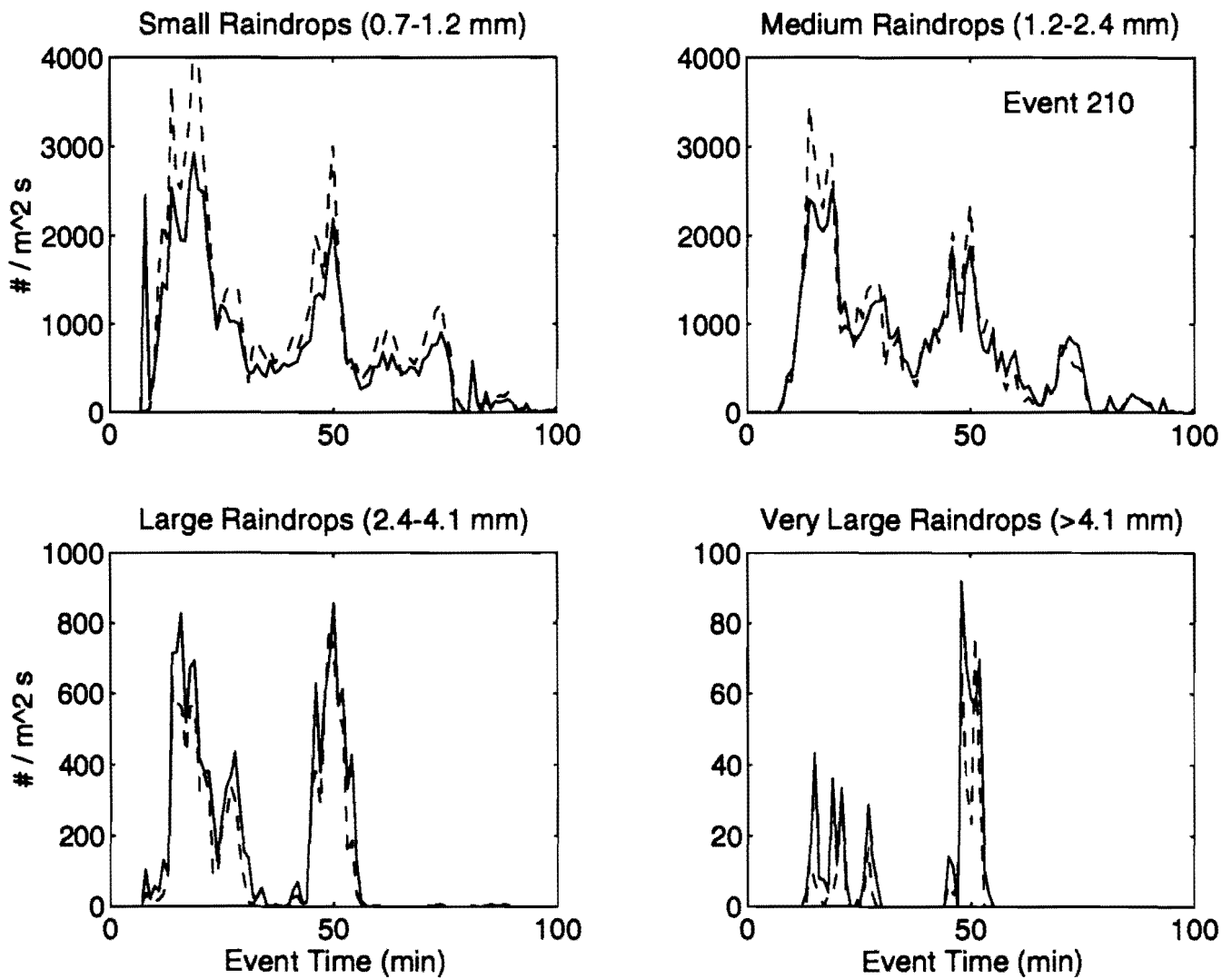


Figure 29. Comparison of drop size category (small, medium, large, and very large) counts for the APL (solid line) and Joss-Waldvogel (dashed line) disdrometers for the rain event of Julian Day 210 (July 29).

## **8. CONCLUSIONS AND RECOMMENDATIONS**

The APL disdrometer performs well when compared to the Joss-Waldvogel disdrometer and a calibrated weighing rain gauge, although both disdrometers underestimate extremely heavy rainfall rates. The APL disdrometer has a more robust sensor element than the Joss-Waldvogel disdrometer and should be deployable in marine environments. It does not have any mechanical elements. Some component changes to the electronics processing circuitry within the APL disdrometer should improve performance. These changes include the use of commercially available IC chips within the demodulator and the computer interface modules. These changes reduce temperature sensitivity, extend the dynamic range of the system, and increase accuracy.

In the future, efforts should be made to reduce the down time associated with individual drop detections. Two improvements are feasible. One, replace the computer interface unit with a high speed digital sampling board within the computer. Software could be designed to do the peak detection, including secondary peaks caused by multiple drop strikes. A second improvement will be to replace the Delrin sensor with a different type of piezoelectric material that has a faster response and recovery time and does not resonate. This material exists. Together these improvements will allow multiple sensor heads to be monitored by a single computer. The net increased sensor area will allow faster temporal sampling of the rainfall drop size distribution.

## **ACKNOWLEDGMENTS**

John Roland and Robert Miller, APL/John Hopkins University, designers of the original APL disdrometer, graciously provided extensive support to this project. They reviewed and updated engineering designs for the APL disdrometer. Donald Mason, NASA Wallops Flight Facility, produced a prototype of the APL electronics circuitry. John Roland checked the prototype boards and then allowed them to be sent to OAD for further evaluation and testing. He also provided comments on the testing performed by OAD.

## APPENDIX A: APL CIRCUIT SOFTWARE

A new software package has been developed to support the APL circuitry. This software controls the data flow from the APL disdrometer into the sampling computer. A user interface display is part of the package. The flow diagram for the software is shown in Figure A1. Critical operations performed by the software include:

- (1) Acquiring the peak voltage value from the Computer Interface Board via a DAS/8 A/D board mounted in the computer.
- (2) Releasing the drop detection flag, allowing additional drops to be detected.
- (3) Converting the voltage value to drop size using the conversion relationship shown in Figure 17.
- (4) Storing the drop size data into selected bin sizes.
- (5) After a selected time interval (currently 1 minute), the bin counts are written into an archive file in the sampling computer.
- (6) Drop size distribution data and selected rainfall parameter, *e.g.*, total rainfall rate, are computed and displayed on the computer monitor.

The software was developed using Microsoft Quick C, Version 2.5. Quick C was selected because of its inherently highly optimized low level communication routines. This allowed the software down time per drop (tasks 1-4 from the list shown above) to be reduced to 1.7 ms (from 7.5 ms). Currently, the data are stored in 20 bin categories (see Table A1), matching the Joss-Waldvogel disdrometer bin sizes. These sizes were selected to facilitate comparison with the Joss-Waldvogel disdrometer. In the future, other size categories can be used, including the selection of a larger number of bins. The current sampling interval is selected to be one minute. Again, this matches the Joss-Waldvogel disdrometer. Shorter sampling intervals can be used in future applications. The optimal sampling interval depends on the actual drop size distribution within the rain, the associated expected drop count in each bin size category, and the surface area of the sensor (50 cm<sup>2</sup>). The data format on the sampling computer archive files is: HHMM BIN1 BIN2 BIN3 ... BIN20, where HH is the hour, MM is the minute, and BIN<sub>*i*</sub> is the number of drops in BIN<sub>*i*</sub> during that minute.

Table A1. Thresholds of drop size bins.

Bin 1:	0.313 mm to 0.405 mm	Bin 11:	1.748 mm to 2.077 mm
Bin 2:	0.405 mm to 0.505 mm	Bin 12:	2.077 mm to 2.441 mm
Bin 3:	0.505 mm to 0.596 mm	Bin 13:	2.441 mm to 2.727 mm
Bin 4:	0.596 mm to 0.715 mm	Bin 14:	2.727 mm to 3.011 mm
Bin 5:	0.715 mm to 0.827 mm	Bin 15:	3.011 mm to 3.385 mm
Bin 6:	0.827 mm to 0.999 mm	Bin 16:	3.385 mm to 3.704 mm
Bin 7:	0.999 mm to 1.232 mm	Bin 17:	3.704 mm to 4.127 mm
Bin 8:	1.232 mm to 1.429 mm	Bin 18:	4.127 mm to 4.573 mm
Bin 9:	1.429 mm to 1.582 mm	Bin 19:	4.573 mm to 5.145 mm
Bin 10:	1.582 mm to 1.748 mm	Bin 20:	>5.145 mm

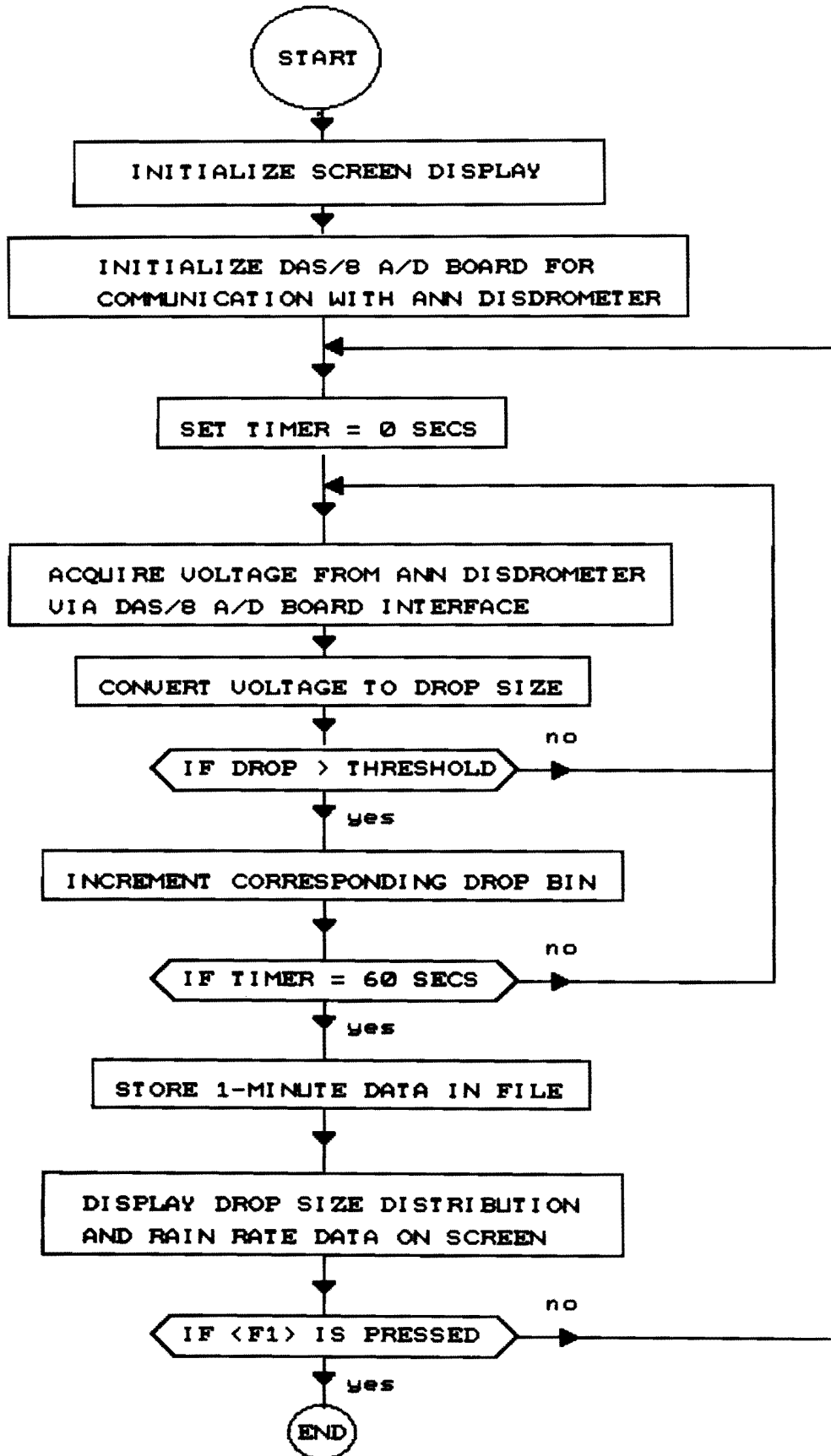


Figure A1. Flow diagram for the new APL circuit software.

## REFERENCES

- Flach, T.E., 1972. An automated system for the measurement and analysis of raindrop size distributions. Masters Thesis, University of Illinois, Urbana, Illinois, Call No. 551.573/F59a.
- Joss, J., and A. Waldvogel, 1969. Raindrop size distribution and sampling size errors. *J. Atmos. Sci.*, 26:566-569.
- Lhermitte, R., 1990. Attenuation and scattering of millimeter wavelength radiation by clouds and precipitation. *J. Atmos. and Oceanic Tech.*, 7:464-479.
- Nystuen, J.A., 1995. Acoustical rainfall analysis: Rainfall drop size distribution using the underwater sound field. *J. Atmos. and Oceanic Tech.* (submitted).
- Nystuen, J.A., J.R. Proni, P.G. Black, and J.C. Wilkerson, 1995. A comparison of automatic rain gauges. *J. Atmos. and Oceanic Tech.* (submitted).
- Pruppacher, H.R., and R.L. Pitter, 1971. A semi-empirical determination of the shape of cloud and rain drops. *J. Atmos. Sci.*, 28:86-94.
- Rowland, J.R., 1976. A comparison of two different raindrop disdrometers. 17th Conference on Radar Meteorology, Seattle, Washington, 398-405.
- Ulbrich, C.W., and D. Atlas, 1978. The rain parameter diagram: Methods and applications. *J. Geophys. Res.*, 83:1319-1325.
- Wang, P.K., and H.R. Pruppacher, 1977. Acceleration to terminal velocity of clouds and raindrops. *J. Appl. Meteor.*, 16:275-280.